INL/RPT-25-87486

Light Water Reactor Sustainability Program

Technical Feasibility Assessment of PWR Core Design for Sizeable Power Uprate

September 2025

U.S. Department of Energy

Office of Nuclear Energy

INL/RPT-25-87486

Technical Feasibility Assessment of PWR Core Design for Sizeable Power Uprate

Carlo Parisi[1]
Robby Christian [1]
Nicholas Rollins[1]
Junyung Kim[1]
Courtney Otani[1]
Chaitee Godbole[1]
Svetlana Lawrence[1]
Mitch Edney[2]
Jason Hou[2]

[1] **Idaho National Laboratory**
[2] **North Carolina State University**

September 2025

Prepared for the
U.S. Department of Energy
Office of Nuclear Energy
Under DOE Idaho Operations Office
Contract DE-AC07-05ID14517

Page intentionally left blank

EXECUTIVE SUMMARY

The federal government of the United States (U.S.) recently identified the establishment of new power generation through the power uprating of existing nuclear reactors as a key aspect of the wider goal to reinvigorate the nuclear sector in the U.S and reliably sustain the growth of artificial intelligence (AI) applications. The Department of Energy (DOE) has been directed to facilitate at least 5 GW of additional energy capacity derived from power uprates of existing nuclear reactors by 2030. To achieve this ambitious goal, a thorough analysis methodology for the existing fleet of light water reactors (LWRs) needs to be developed. This new methodology will evaluate with reduced conservativisms new core designs and their corresponding safety margins. In this report, we present the scheme and the preliminary application of such methodology.

This report outlines the feasibility study conducted for a significant power uprate of a pressurized water reactor (PWR) by using low 5%–10% enrichment uranium (LEU+) fuel at high burnup. The study focuses on the South Texas Project (STP) Unit 1 reactor and employs advanced computational tools including the PARCS, POLARIS, and RELAP5-3D codes to perform core neutron transport calculations, transient system modeling, and safety analyses of an aggressive power-uprated core. This report serves as a critical step in demonstrating the viability and benefits of power uprates, paving the way for reinvigoration of the U.S. nuclear sector.

Key findings in fiscal year 2025 (FY-25) include the successful optimization of the STP Unit 1 reactor core with the application of an extended power uprate to 4500 MW_{th}, up from 3800 MW_{th}, as well as a lengthening of the fuel cycle to 24 months. This was achieved while meeting all design and safety criteria, including thermal power peaking factors and peak soluble boron concentration in the coolant. Fuel assembly models for the 17×17 fuel lattice were created using the POLARIS code to generate a multiparametrized cross-section library with the addition of LEU+ fuel and urania-gadolinia burnable poisons to support the significant increase in thermal power (18%). The STP Unit 1 reactor core was then optimized to support the extended power uprate and to include the new LEU+ fuel designs. Then, a reactor system model was developed using RELAP5-3D to analyze the power-uprated core configurations at system level. The RELAP5-3D model is an STP Westinghouse four-loop model, with a high-fidelity core nodalization (each fuel assembly is independently modeled). Moreover, the model uses the three-dimensional nodal kinetics calculation of the RELAP5-3D code to obtain detailed fuel assembly power distribution. A methodology was developed and validated to automatically import the POLARIS cross section database and PARCS optimized core scheme in RELAP5-3D. A sample transient of a rod ejection accident (REA) was created to demonstrate the tool capabilities, with additional anticipated operational occurrence (AOO) and design basis accident (DBA) scenarios planned for the coming fiscal year. Finally, a methodology for coupling RELAP5-3D with CTF subchannel code has been derived. All these activities result in a definition of a complete computational platform that can be used, in conjunction with a risk-analysis tool like RAVEN (Risk Analysis and Virtual Environment), to perform best estimate plus uncertainty (BEPU) analysis of the safety margins of the power-uprated cores.

Page intentionally left blank

CONTENTS

FIGURES

TABLES

Page intentionally left blank

ACRONYMS

AOO	Anticipated Operational Occurrence
ATF	accident tolerant fuel
BEPU	Best Estimate Plus Uncertainty
BOC	beginning of cycle
CTF	COolant Boiling in Rod Arrays-Two Fluids
DBA	design basis accident
DOE	Department of Energy
EFPD	Effective Full Power Day
EOC	end of cycle
EPU	Extended Power Uprate
FY	Fiscal Year
IFBA	integral fuel burnable absorber
LEU	Low 0%–5% Enrichment Uranium
LEU+	Low 5%–10% Enrichment Uranium
LWR	light water reactor
MUR	Measurement Uncertainty Recapture
NRC	Nuclear Regulatory Commission
PARCS	Purdue Advanced Reactor Core Simulator
PWR	pressurized water reactor
RAVEN	Risk Analysis and Virtual Environment
REA	Rod Ejection Accident
RELAP	Reactor Excursion and Leak Analysis Program
R&D	Research and Development
SPU	Stretch Power Uprates
STP	South Texas Project

Page intentionally left blank

1. INTRODUCTION

The federal government of the United States (U.S.) recently identified the establishment of new power generation through the power uprating of existing nuclear reactors as a key aspect of the wider goal to reinvigorate the nuclear sector in the U.S. In May 2025, President Trump signed an executive order directing to "Facilitate the expansion of American nuclear energy capacity from approximately 100 GW in 2024 to 400 GW by 2050" [1]. Another Executive Order directed the Department of Energy (DOE) to "facilitate 5 gigawatt of power uprates to existing nuclear reactors by 2030" [2]. This ambitious goal implicates a monumental degree of engineering effort to optimize fuel designs, select new fuel inventories, and redesign fuel reloading schemes for a large number of nuclear power plants. Currently, a clear methodology and understanding of how to effectively, economically, and safely apply larger-than-historically-accomplished extended power uprates (EPU), in this report referred to as EPU+, to the existing fleet of light water reactors (LWRs) is not well established.

Over the past few decades, there have been many power uprates approved by the Nuclear Regulatory Commission (NRC) resulting in a total increase of 22,560 MW_{th} [4]. Historically, there are three types of power uprates implemented in the U.S.: Measurement Uncertainty Recapture (MUR) power uprates, Stretch Power Uprates (SPU), and EPUs. MUR power uprates consist of reclaiming a fraction of the 2% uncertainty factor to thermal power calculations specified in 10 CFR 50 Appendix K to account for uncertainty in feedwater flow. This uncertainty reduction can result in an increase of reactor licensed thermal power between 1% and 2% and can be achieved by implementing improved thermal power calculation techniques. SPUs typically are power uprates between 2% and 7% and are achieved by use of the original design's excessive safety margins to accommodate an increase in thermal power. These original demonstrated safety margins can be increased through improved predictions of core behavior with modern simulation techniques or additional experimental data to reduce uncertainty. EPUs refer to larger increases in thermal power beyond 7%, though typically not exceeding 20%. EPUs often require major modifications to significant number of balance-of-plant components such as the high-pressure turbines, condensate pumps and motors, main generators, transformers, and others.

There are several additional ways to support plant power increases, including the application of novel fuel designs capable of enduring the uprated operating conditions, such as accident tolerant fuel (ATF) designs, or higher enriched fuel capable of providing the additional energy to be extracted during the uprated fuel cycle, such as low-enriched uranium with higher enrichment (LEU+) fuel, or risk-informed transient analyses of design basis accidents (DBAs), such as loss of coolant accidents (LOCAs) or reactivity insertion accidents . ATF designs can enhance safety at U.S. nuclear power plants by offering superior performance during normal operation, transient conditions, and accident scenarios, especially in high-burnup conditions. Combining these advanced fuel designs with increased enrichments up to 10%, LEU+ can boost operational flexibility, enable the extension of fuel cycles, and support EPU+s. Risk-informed analysis of DBAs also helps identify and mitigate potential vulnerabilities of the uprated core design, enhancing the reliability and efficiency of power uprates. Lastly, an extended fuel cycle supports power uprates by improving fuel efficiency and reducing refueling frequency. Utilizing high-burnup fuel and optimizing fuel management and reloading strategies allows the plant to sustain increased power levels for longer periods, minimizing operational interruptions, improving the reliability of energy supplied to the grid, lowering fuel costs, and maximizing economic performance.

This project aims to conduct a feasibility study for a significant power uprate to a pressurized water reactor (PWR) by using 5%–10% enrichment LEU+ fuel at high burnup. Performance and safety analyses of various power uprate approaches will be evaluated and compared in a multiphysics context, considering reactor physics, thermal-hydraulics, fuel performance, and economics using state-of-the-art computational codes.

In fiscal year 2025 (FY-25), research and development (R&D) focused on demonstrating the application of an extended power uprate to a high-fidelity core model of an existing PWR core design operating in the U.S.; the South Texas Project (STP) Unit 1. The Purdue Advanced Reactor Core Simulator (PARCS) [5], the U.S. NRC licensing tool for solving the time-dependent multigroup neutron diffusion equation in three-dimensional Cartesian geometry, was employed to perform core transport calculations before and after the application of the extended power uprate, ensuring the study's relevance to the nuclear industry and accelerating the licensing process with the identified optimal design approach. Fuel assembly models for the 17×17 fuel lattice were created to generate a multiparametrized cross-section library using the POLARIS code [13]. This process was repeated with the addition of LEU+ fuel and urania-gadolinia burnable poisons to support the significant increase in thermal power. The STP Unit 1 reactor core was then optimized to support the extended power uprate and to include the new LEU+ fuel designs.

The report is organized as follows: Section 2 provides a demonstration of the fuel design and optimization necessary to apply a significant power uprate to an existing LWR with all necessary considerations made to fuel performance, economics, multicycle operation, and safety. Section 3 presents the RELAP5-3D [3] system models of STP and the results of the rod ejection accident analysis, and briefly the conceptual methodology created to further improve the fidelity of these simulations at a pin-resolved level using an external coupling scheme with the subchannel thermal hydraulics code CTF. Section 4 concludes the study and outlines potential future work.

2. DEMONSTRATION OF POWER UPRATES METHODOLOGY

2.1 Reactor Core Model: South Texas Project Unit 1

The extended power uprate demonstrated in this work was applied to the STP Unit 1 PWR reactor design [19]. The design of this reactor core includes a 14-foot (4.27 meters) fuel assembly-based core. The reactor vessel is constructed of 304 Stainless Steel (SS304) and is cooled by water doped with soluble boric acid. Axial neutron reflectors, each 10 inches (25.4 cm) tall, are placed above and below the active region of the core in the coolant flow. The fuel assembly designs include urania (UO_2) fuel enriched to either 4.2% or 4.6% ^{235}U by weight. Fresh fuel reactivity is controlled by the inclusion of integral fuel burnable absorber (IFBA) coated fuel rods. The fuel assemblies enriched to 4.2% ^{235}U include three configurations of the IFBA fuel rod loading with 64, 105, and 128 IFBA rods, respectively. The fuel assemblies enriched to 4.6% ^{235}U only use the 128 IFBA fuel rod loading configuration, for a total of four fuel assembly designs loaded into the core. IFBA fuel rods are manufactured by coating standard UO_2 ceramic fuel pellets with a very thin coating (~26 μm) of zirconium diboride (ZrB_2). The boron serves as a burnable neutron poison, while the ZrB_2 itself has favorable mechanical and thermophysical properties that allow it to minimally impact the performance of the fuel pellet.

Each of the four fuel assembly designs utilize the same axial configuration. The total height of the fuel assemblies is 168 inches (426.7 cm). Eight inches (~20 cm) of the fuel assembly height are reserved at both the top and bottom of each rod for a "blanket" region, wherein the UO_2 fuel is enriched to 2.6% by weight. No IFBA coating is included in the blanket region for any of the fuel assembly designs. The radial layout for the three IFBA loading configurations, as well as the axial enrichment configuration, is detailed in Figure 1..

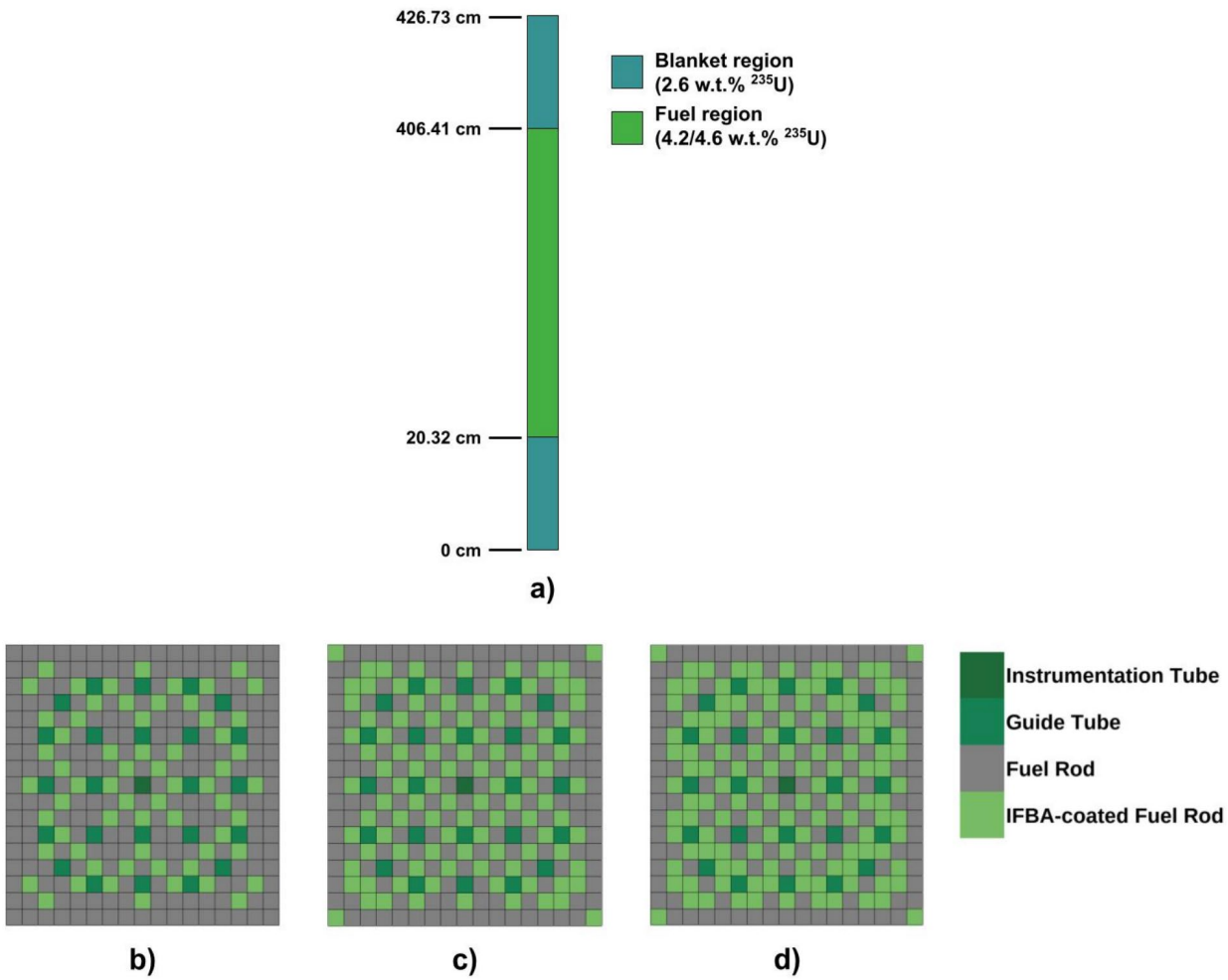

Figure 1. (a) Axial enrichment regions of the fuel assemblies; and the radial layout of the STP 17 × 17 fuel assemblies: (b) 64 IFBA, (c) 108 IFBA, and (d) 124 IFBA.

Each fuel assembly contains a 17 × 17 array of pins. Of these, 264 contain UO_2 fuel. The center rod is reserved as an instrumentation tube for scientific measurements as needed. Twenty-four guide tubes are situated throughout the fuel assembly to serve as pathways for the insertion of control rods. The geometric specifications for the fuel assembly designs are summarized in Table 1.

Table 1. STP model fuel assembly specifications.

Specification	Value
Fuel rod array	17 × 17
UO_2 rods	264
Guide Tubes	24
Instrumentation Tubes	1
Fuel density (g/cm^3)	10.412
Assembly pitch (cm)	21.50
Rod pitch (cm)	1.26
Overall dimensions (cm × cm)	21.402 × 21.402

The cross section libraries were generated using the lattice physics code POLARIS [13]. Each type of fuel assembly described previously was modeled as a two-dimensional (2D) lattice under various conditions of fuel and coolant temperature, coolant density, boron concentration, and control rod insertion to capture the range of conditions in each of these state variables that might be expected during nominal operation or could arise as the result of safety-related transients. At each set of conditions, macroscopic multigroup cross sections for the homogenized fuel assembly were generated and concatenated to form a complete case matrix cross section library. Each lattice physics calculation was conducted to 23 depletion timesteps for a total burnup of 80 GWd/MTU at a nominal reactor power of 36 W/g_{IHM}.

The cross sections were generated in POLARIS using nuclear data taken from a 252-group library derived from the ENDF/B VII.1 database. These are generated in the '.t16' file format as two-group macroscopic cross sections, and in the '.PMAXS' file format using the code GenPMAXS, allowing for use in PARCS and TRACE [7].

An equilibrium cycle shuffling scheme was created for the STP Unit 1 reactor core to use as a pre-uprated comparison. The equilibrium cycle is defined as a steady-state fuel cycle where the fuel loading, burnup distribution, and reactivity characteristics remain consistent from cycle to cycle of repeated operation. Essentially, once an equilibrium cycle is reached, each new cycle appears identical to the previous cycle in terms of fuel performance, power distribution, and irradiation history throughout the cycle. This makes it an ideal point of comparison to demonstrate the viability of an extended power uprate as it demonstrates sustainable behavior through multiple consecutive operating cycles. The reference equilibrium cycle shuffling scheme and the resulting core performance characteristics are presented in Figure 2 and Table 2, respectively.

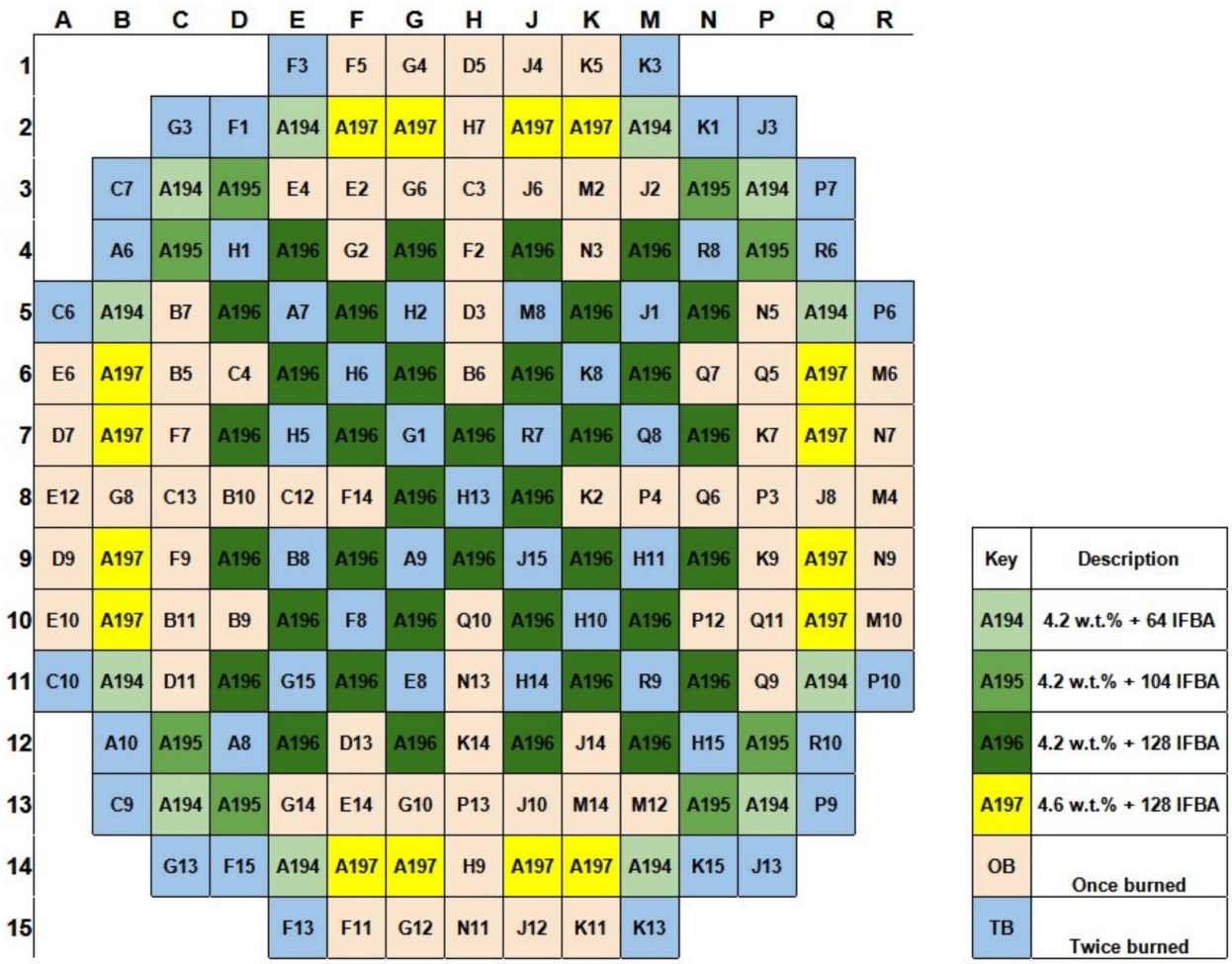

Figure 2. Equilibrium cycle reference solution for the STP reactor core design.

Table 2. STP model reference solution performance summary.

Objective	Value
Power Uprating (MW_{th})	3,800
Max. Cycle Length (Effective Full Power Day [EFPD])	392.84
Maximum Soluble Boron (ppm)	893.6
Beginning of Cycle (BOC) Core-averaged Exposure (GWd/MTU)	19.53
EOC Peak Exposure (GWd/MTU)	71.52
F_Q	2.141
$F_{\Delta H}$	1.588

2.2 Application of Extended Power Uprates and 24-Month Cycle

The goal of the present work is to explore the viability of ambitious power uprates applied to currently operating nuclear reactors. To this end, the goal of this optimization targets an extended power uprate of more than 18%, representing an increase in thermal power production from 3800 MW_{th} to 4500 MW_{th}, with a simultaneous cycle lengthening from 18 months (530 effective full power days

[EFPD]) to 24 months (700 EFPD). The associated thermohydraulic changes necessary to facilitate this extended power uprate are summarized in Table 3.

Table 3. Operating conditions of the STP reactor model before and after extended power uprates.

Parameter	Nominal Value	Uprated Value
Power Uprate	0.00%	18.42%
Power Rating (MW_{th})	3,800	4,500
Core Inlet Mass Flow (kg/s)	19,822	23,473
Core Inlet Temperature (K)	566.5	566.5
Core Outlet Temperature (K)	599.5	599.2

Between the cycle lengthening from 530 EFPD to 700 EFPD and power uprating proposal of 18.4%, these changes represent a drastic increase in the amount of nuclear energy being extracted from the fuel inventory in each cycle. The previous selection of four fuel assembly types consisted of three fuel assembly types containing 4.2% enriched UO_2 fuel and 64, 104, and 128 IFBA fuel rods, respectively, along with a fourth fuel assembly type containing 4.6% enriched UO_2 fuel and 128 IFBA fuel rods, following the designs for the IFBA fuel rod layout described in Figure 1. This configuration will not provide the necessary initial heavy metal loading necessary to reach these new design goals. To address this issue, new fuel assembly types will be proposed containing fuel enrichments in the LEU+ range, specifically between 5 wt% to 10 wt% ^{235}U.

There are potential drawbacks or complications that arise from increasing the enrichment of the fuel used in a nuclear reactor. Apart from the potential for increased nonproliferation-related concerns, which are outside the scope of the present work, a nuclear fuel with an increased enrichment of fissile material will be more neutronically active in the presence of the same radiation flux. This effect can often be counteracted by proportionally increasing the presence of burnable poisons via dedicated control elements and through soluble boric acid. One impact that is not so easily mitigated, however, is the increased cost associated with fabricating a higher enriched nuclear fuel.

Increasing the fuel enrichment from LEU to LEU+ is expected to result in a much larger beginning of life (BOL) reactivity. The use of IFBA fuel rods in the fuel assembly designs described previously is intended to address the concern of high BOL reactivity, as the IFBA material serves as a burnable neutron poison that is consumed in relatively short order during the operating cycle, usually within ~10 GWd/MTU of burnup. Thus, its impact is observed exclusively at the BOL of the fuel assembly. The layout with the highest loading of burnable poison, 128 IFBA fuel rods, is not expected to be adequate to offset the much larger BOL reactivity associated with LEU+ fuel. However, this discrepancy will be addressed in a following section and 128 IFBA fuel rods will be assumed for the purposes of the initial analysis with the remaining excess reactivity in the core being offset by an elevated, though unfeasible, concentration of soluble boron in the coolant.

The resulting solution identified by the optimization of the equilibrium cycle in MIDAS after the power uprate of the STP reactor core successfully meets all the design criteria, including the 700 EFPD cycle length goal and 4500 MW_{th} uprated power output, and is depicted in Figure 3. It is difficult to make a direct comparison between the equilibrium cycle reference solution and the new uprated optimized solution using the shuffling scheme alone due to the differences in the composition of the fuel inventory. There is a notable distinction in the apparent haphazard nature with which the fuel is loaded into the core in the uprated solution compared to the highly ordered approach of the reference solution. This is a hallmark of the MIDAS framework, which is used to optimize the equilibrium cycle shuffling scheme and is typical of optimization methods like it. The success of these methods is evident in the relative performance of the resulting solutions despite the seeming arbitrary nature of the fuel distribution in the shuffling scheme.

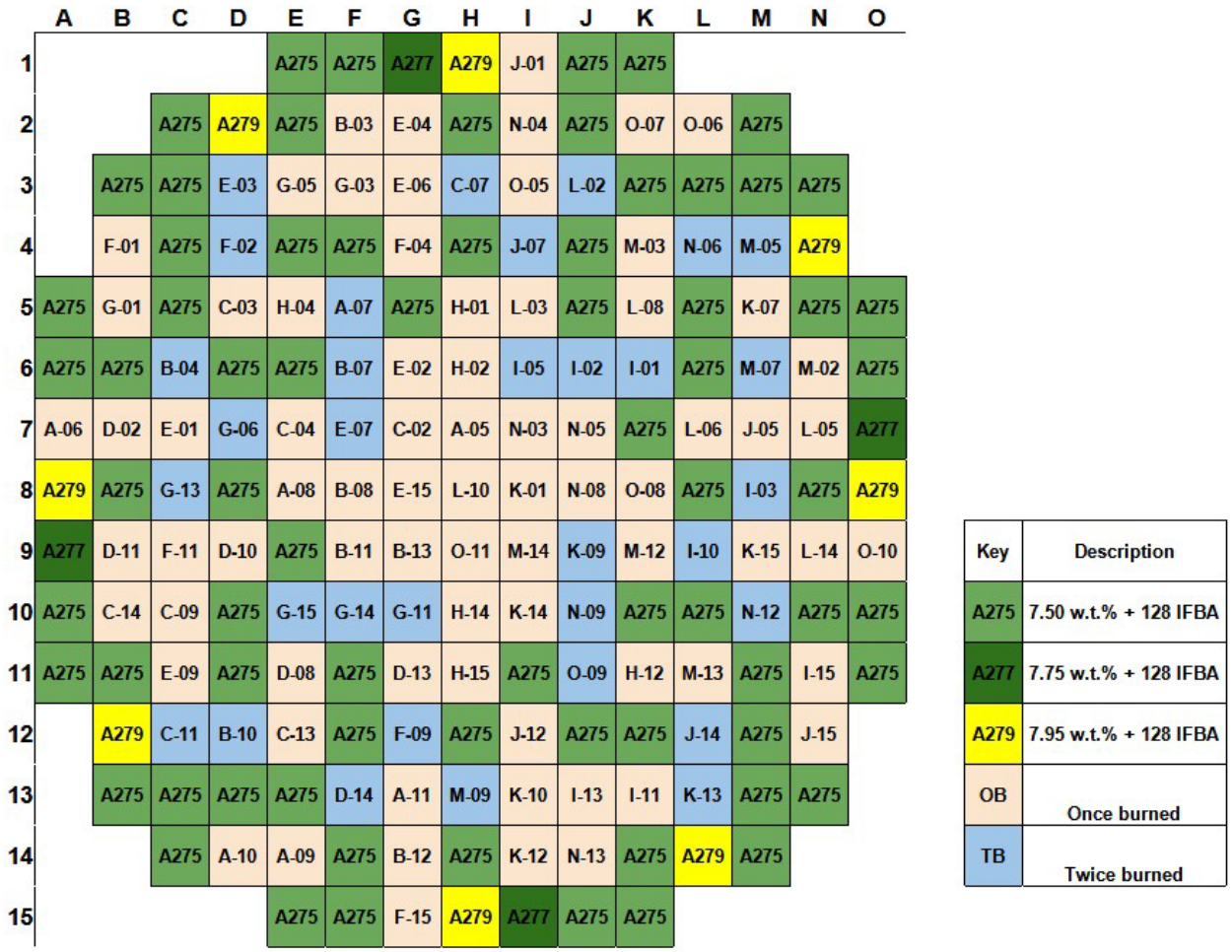

Figure 3. EQ cycle optimized solution for the STP reactor core power uprates.

Table 4. Optimized solution performance for STP model with power uprates.

Objective	Value	Limit
Max. Cycle Length (EFPD)	718.86	700.00
Max. Soluble Boron (ppm)	2678.4	1800.0
BOC Core-averaged Exposure (GWd/MTU)	22.47	
EOC Peak Exposure (GWd/MTU)	97.05	
F_Q	1.944	2.100
$F_{\Delta H}$	1.492	1.650

As previously noted, the increase in fuel enrichment from LEU to LEU+ is accompanied by a significant rise in soluble boron concentration in the coolant, even though this was minimized as part of the optimization process. The goal of a 700 EFPD maximum cycle length was accomplished with the power uprates optimized solution reaching a cycle length of 718.86 EFPD. This represents a 48.4% increase from the previous optimized solution cycle length and an 83.0% increase from the reference solution cycle length, on top of the 18.4% power uprate in thermal power output. As expected, operating the reactor at such an elevated power rating for a long duration results in an unrealistic end-of-cycle

(EOC) peak exposure value of 97.05 GWd/MTU. This far exceeds the limit for peak fuel rod exposure set by the NRC, which is expected because minimizing this value is not an objective in this work scope. This regulatory limit will be increased in the future to 75 or even 80 GWd/MTU with the inclusion of Accident Tolerant Fuel (ATF) concepts. This would certainly make the expected EOC Peak Exposure value of the power uprates optimized solution appear more viable, but the inclusion of ATF concepts is outside the scope of the present work.

One solution to the problem of high cycle exposures resulting from power uprates would be to replace the most burned fuel assemblies at the EOC (which are in the twice-burned batch) with fresh fuel assemblies, both decreasing the amount of burnup in the core as well as increasing the margin for additional burnup that can be added to the core over the course of the cycle. This is not an ideal solution, however, as increasing the size of the feed batch in this way is often seen as an unnecessary addition to the fuel cycle cost. In either case, there is a larger-than-normal gradient of burnup values that remain in the core between the feed batch and twice-burned batch, even at EOC. Unless the core deviates significantly from a three-batch fuel cycle, this can simply be viewed as a symptom of the 24-month fuel cycle that is only exacerbated by the extended power uprate.

2.3 Reactivity Control Using Urania-Gadolinia Fuel

2.3.1 Fuel Design with Urania-Gadolinia

Increasing the fuel enrichment from LEU to LEU+ results in a much larger BOL reactivity which, if unaddressed, must be counteracted by a proportional increase in soluble boron concentration in the coolant. There is a limit to the concentration of soluble boron that can be safely loaded into the reactor coolant. Using boric acid increases the acidity of the water coolant, increasing the rate of corrosion of the structural materials in the reactor. Furthermore, high concentrations of ^{10}B in the water coolant can lead to instabilities in the moderator temperature reactivity feedback that may jeopardize the safe operation of the reactor core [8, 9]. The use of IFBA fuel rods in the fuel assembly designs described in Figure 1 is intended to address the concern of high BOL reactivity, as the IFBA material serves as a burnable neutron poison that is consumed in relatively short order during the operating cycle, usually within ~10 GWd/MTU of burnup. Thus, its impact is observed exclusively at the BOL of the fuel assembly.

Considering the performance of the uprated solution discussed previously, it is evident that the 128 IFBA fuel rods layout described in Figure 1 is not sufficient to control the BOL reactivity introduced by the LEU+ fuel enrichments. IFBA fuel rods are manufactured by coating standard UO_2 ceramic fuel pellets with a very thin coating ZrB_2. This makes the IFBA fuel rod concept highly versatile, but the thin coating offers only a limited amount of reactivity control. A more effective, but more intrusive, form of reactivity control is to introduce gadolinia (Gd_2O_3) into the fuel pellet itself. Typically, this is done at a relatively low weight percent of gadolinia (<10%). When the two ceramics are mixed to form the urania-gadolinia fuel pellet, it is common for a lower enrichment of ^{235}U to be used to address concerns related to thermal conductivity and reactivity control. The urania-gadolinia mixture has a lower thermal conductivity than the typical UO_2 ceramic material, leading to higher temperature gradients within the fuel pellets. A ^{235}U enrichment reduction in gadolinia-bearing fuel pellets lowers the thermal power output in the fuel rod in question, mitigating the risk of localized overheating. The urania-gadolinia fuel pellets are manufactured to the same dimensions as typical UO_2 ceramic fuel pellets. Coupled with the ^{235}U enrichment reduction in gadolinia-bearing fuel pellets, this means that, unlike with the IFBA concept, the use of gadolinia as a burnable poison for reactivity control necessarily has the unintended effect of decreasing the initial heavy metal loading of the reactor core. Minimizing the quantity of gadolinia-bearing fuel introduced into the reactor mitigates this impact [10, 11].

It has also been proposed to enrich the gadolinium in the gadolinia prior to the manufacturing of the fuel material, either to 100% ^{155}Gd or 100% ^{157}Gd. This has been found to have a favorable impact on the

ability of the poison to control BOL reactivity but can contribute to higher pin power peaking in the fuel assembly and presents an additional expense in the manufacturing of the fuel assembly [12]. Enriched gadolinia will not be considered for the purposes of the present work.

Of particular concern when considering the design of fuel assemblies loaded with neutron poisons is the maximum relative power peaking observed in the fuel lattice. To validate the fuel assembly design layouts proposed in this work, 2D fuel lattice calculations were performed using the lattice physics code POLARIS from the SCALE code package [13]. From these calculations, the relative power distribution was analyzed. The present work imposed a maximum pin relative power peaking value of 20% above nominal.

Following these considerations, a number of gadolinia-bearing fuel assembly configurations were created, with varying quantities of burnable absorber rods and gadolinia loadings. In each of these proposed configurations, the fuel enrichment of the axial "blanket" region at the top and bottom of the fuel assembly was increased from 2.6% to 4.95% ^{235}U by weight. As with the IFBA coatings, no gadolinia burnable poison was included in the axial blanket region. The best fuel assembly design, dubbed "M8," was selected for use in the present work and is depicted in Figure 4. The maximum pin relative power peaking value for the "M8" design is 17.2%.

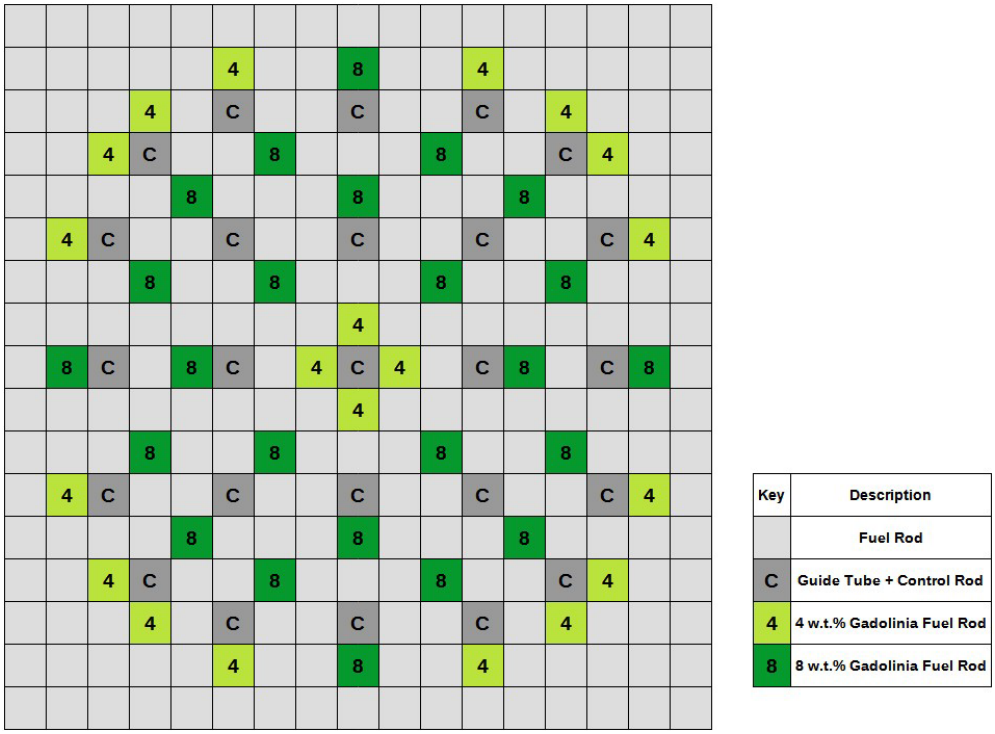

Figure 4. Gadolinia-bearing fuel assembly design layout: M8.

As previously mentioned, a reduction in the ^{235}U enrichment in gadolinia-bearing fuel pellets is commonly implemented to counteract the lower thermal conductivity of the urania-gadolinia mixture. This was assumed in the present work to take the form of a 5% relative reduction in ^{235}U enrichment for each percentage point of concentration of Gd_2O_3 by mass included in the urania-gadolinia mixture. The resulting ^{235}U enrichment is summarized in Table 5.

Table 5. Reduced ^{235}U enrichment for various gadolinia concentrations and LEU+ enrichments.

Nominal ^{235}U Enrichment	**Reduced ^{235}U enrichment**	
	Concentration of Gd_2O_3-bearing rods	
	4 wt%	8 wt%
7.50%	6.00%	4.50%
7.75%	6.20%	4.65%
7.95%	6.36%	4.77%

2.3.2 Extended Power Uprates with Urania-Gadolinia Fuel

With the inclusion of the power uprates goals of achieving a 700 EFPD cycle length at an operating power of 4500 MW_{th} and use of the selected gadolinia-bearing fuel assembly configuration dubbed "M8," the STP Unit 1 reactor core was reoptimized using the MIDAS framework.

Including urania-gadolinia fuel into the STP reactor core addresses the concern of uncontrolled excess reactivity at beginning of cycle (BOC) that results from the increase in fuel enrichment from LEU to LEU+, which is required to drive the uprated power output for the intended operating duration. In the previous analysis, this was accomplished by increasing the soluble boron concentration in the reactor coolant beyond safe levels. The following analysis will therefore include the additional primary objective of reducing the peak critical soluble boron concentration to below 1,800 ppm while minimizing the fuel cycle cost.

The resulting solution identified by the optimization of the equilibrium cycle in MIDAS with the inclusion of gadolinia-bearing fuel assemblies in the STP reactor core successfully meets all the design criteria, including the additional criterion to reduce the soluble boron concentration below 1,800 ppm, and is depicted in Figure 5. The PARCS internal one-phase mass-energy solver was employed for thermal-hydraulic feedback for the purposes of equilibrium cycle convergence.

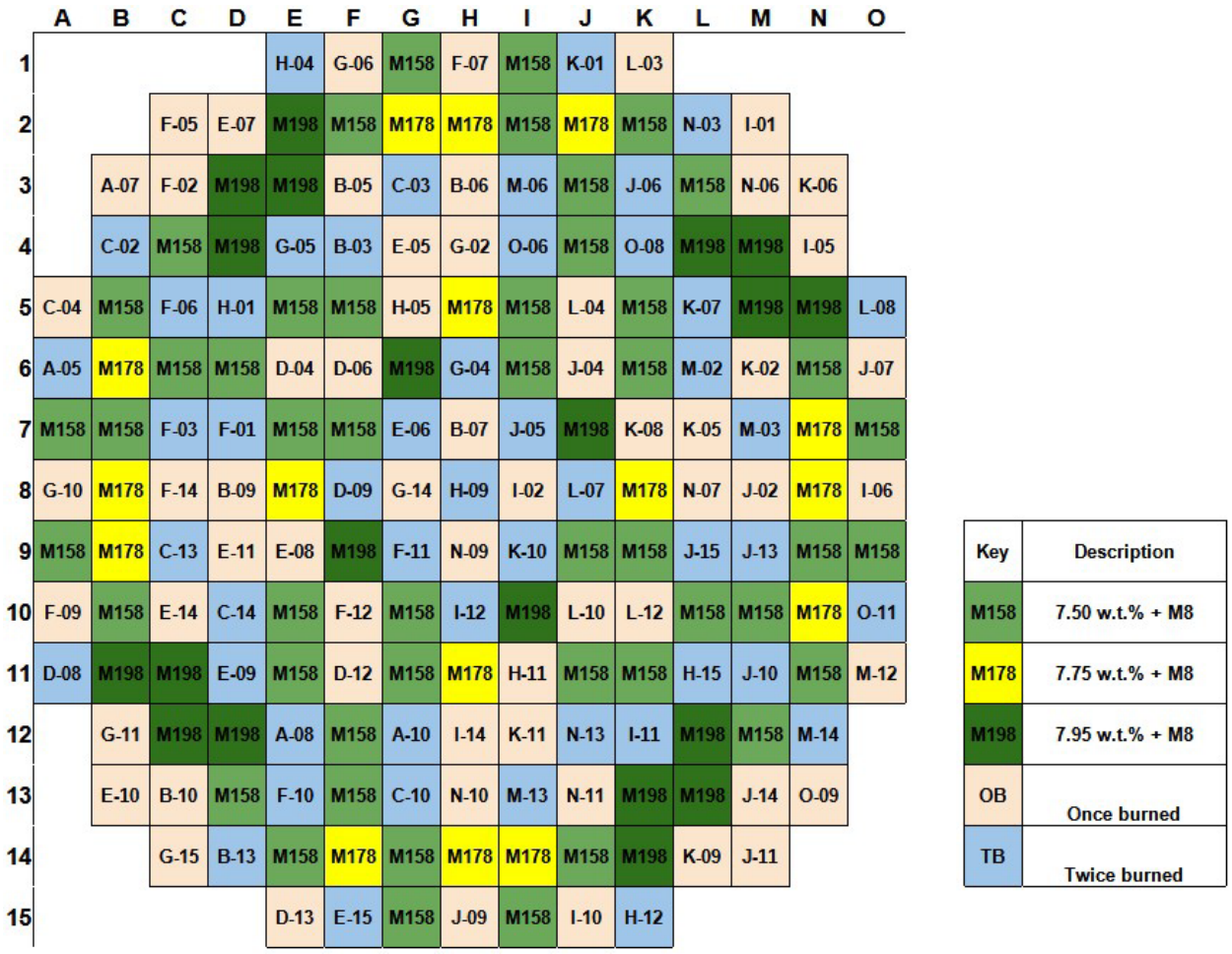

Figure 5. Equilibrium cycle optimized solution for the STP reactor with UO_2-Gd_2O_3 fuel.

The "M8" fuel assembly design configuration includes a large gadolinia loading. This assists in effectively controlling the BOC core reactivity, enabling a greatly reduced soluble boron concentration to be used in the reactor coolant. It should be noted that the burnable poison in the Gd_2O_3 material is fully consumed by ~25 GWd/MTU. Therefore, none of the fuel assemblies in the once- or twice-burned batches contribute any reactivity control through Gd_2O_3. The size of the feed batch and once-burned batch are each 84 fuel assemblies with the twice-burned batch making up the balance of the core, corresponding to a 2.3 region core. The resulting target values of this optimized solution with power uprates are outlined in Table 6.

Table 6. STP model with urania-gadolinia fuel optimized solution performance summary.

Objective	Value	Limit
Max. Cycle Length (EFPD)	702.66	700.00
Max. Soluble Boron (ppm)	1771.1	Minimize
BOC Core-averaged Exposure (GWd/MTU)	22.74	
EOC Peak Exposure (GWd/MTU)	98.39	
F_q	2.055	2.100
$F_{\Delta H}$	1.554	1.650

The transition of optimization objectives, from maximizing the maximum cycle length to minimizing the peak soluble boron concentration, is observed in the urania-gadolinia-optimized solution maintaining maximum cycle length of just over the limit of 700 EFPD, which is required to reach the 24-month fuel cycle while significantly decreasing the peak soluble boron concentration to 1771.1 ppm, a reduction of 33.9% from the previous optimized solution.

Maintaining a maximum cycle length as close to the limit of 700 EFPD as possible was necessary to guide the inclusion of gadolinia in the feed batch while minimizing the resulting increase in the fuel cycle cost. The resulting average fuel enrichment of the feed batch is comparable to that of the power uprates optimized solution of 7.80 wt% ^{235}U. The EOC Peak Exposure value of 98.39 GWd/MTU exceeds the limit for peak fuel rod exposure set by the NRC [14]. Reducing the peak exposure value in the reactor core would likely require increasing the size of the feed batch in the equilibrium cycle shuffling scheme. This would increase the cost of the fuel cycle, but would not sacrifice the optimized solution performance in the other optimization objectives, such as soluble boron concentration and maximum cycle length.

2.4 Further Core Optimization with Extended Power Uprate

2.4.1 Refinement of Urania-Gadolinia Fuel Designs

The inclusion of numerous fuel designs significantly broadens the decision space for core loading pattern optimization. To reduce the size of this decision space, the optimizer's selection was limited to two gadolinia-loading pattern designs, or fuel designs. The fuel designs evaluated for refinement included enrichments of 7.5%, 7.75%, and 7.95%. Each enrichment had fuel loading designs with varying gadolinia loadings and placement, such as the M1, M2, M3, M4, M8, and M9 layout designs. The layout design labeled "N" contained no gadolinia and was used as a reference for the fuel assembly performance. Validation of the fuel assembly designs were conducted in the same manner as described in the prior section.

An initial screening of these fuel designs focused on their ability to maintain criticality throughout the equilibrium cycle. A 0-D core model was employed to assess this capability, assuming a flat power distribution, even batch sizes, and a single fuel assembly design for the core. The EOC for the 0-D core model was determined based on the cycle burnup of a three-region core. The cycle burnup accounted for performance standards of 4500 MWth power output and a 24-month operating cycle. Burnup increments for three cycles were attributed to their respective regions. The expected burnup for each region was then applied to the fuel designs' infinite multiplication factor (k_{inf}) curves to interpolate the k_{inf} values at the expected EOC burnup for each region.

Among the evaluated options, the fuel designs with 7.95% enrichment exhibited the highest EOC multiplication factors when compared to designs with similar loading configurations, while the M4 fuel design performed best compared to other layouts, as shown in Figure 6. To further reflect system realities, a non-leakage probability was incorporated. Previous system simulations indicated a leakage rate of approximately 4%; however, a conservative estimate of 6% was applied for further analysis. Fuel designs that failed to meet this leakage threshold were considered incapable of maintaining criticality for the full cycle duration under the assumptions of the 0-D model.

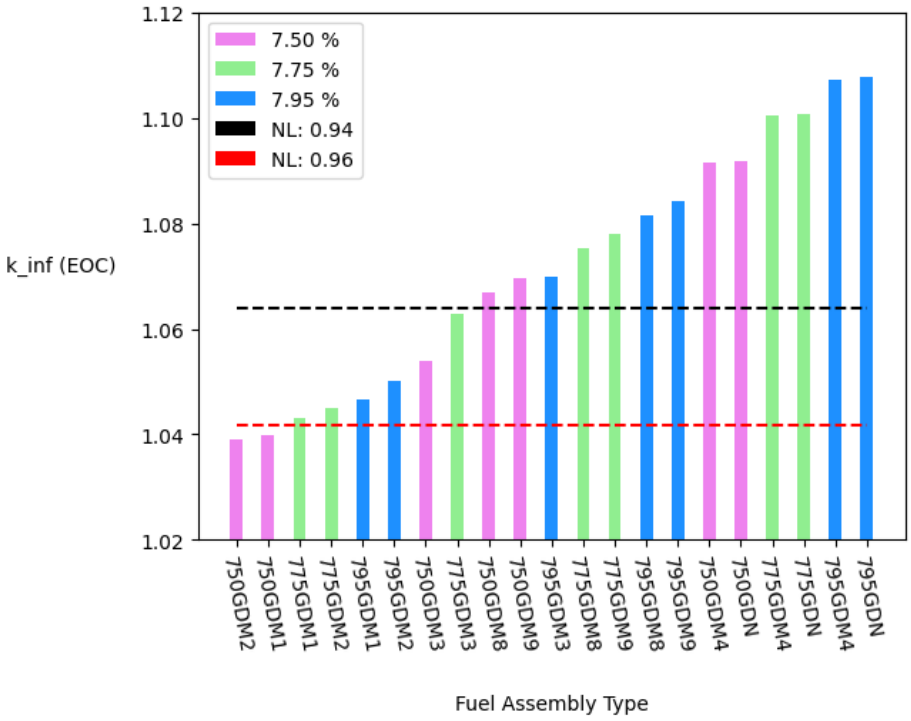

Figure 6. Zero-D model of core multiplication factor at EOC for one fuel assembly type.

Assuming a linear relationship exists between the combined multiplication factor of two fuel assemblies within a two-fuel design core, a combination consisting of one assembly below the leakage threshold and one assembly above the leakage threshold will achieve a sufficient multiplication factor at EOC. These two assemblies are referred to as the "high-reactivity" fuel design and the "low-reactivity" fuel design. Such pairings of fuel designs were selected for further evaluation because of their ability to meet the criticality requirement for the cycle length and to aid in mitigating power peaking. Combinations where both fuel designs were either above or below the threshold were excluded due to the risk of excessive or insufficient reactivity, as indicated by the 0-D model.

To refine the selected fuel design pairings, a linear programming (LP) model was employed. The LP model provides a computationally efficient method for identifying goal-oriented designs that satisfy physical constraints, based on the linear assumption derived from the 0-D model. The LP was formulated as an optimization problem to determine the most desirable fuel design pairings aligned with the established objectives. For each selected pairing, the decision variables represented the number of assemblies of each fuel design allocated to each region. The constraints incorporated physical requirements such as realistic batch sizes and maintaining criticality. The LP was optimized for each pairing at core feed region sizes ranging between 2 and 3. The minimum feed region size that satisfied the criticality constraint was determined to be 84.

One leading objective of the optimization was to minimize the deviation from criticality in the core at EOC for each pairing, thereby eliminating design pairings with the potential for significant excess reactivity throughout the cycle. Pairings that achieved higher multiplication factor values at the minimized criticality deviation were prioritized, as they provided greater assurance of maintaining criticality for the target cycle length. Although not explicitly specified as a goal, the amount of gadolinia loaded was also considered since gadolinia plays an important role in controlling BOC reactivity and core boron concentration.

The most favorable pairings resulting from this analysis included the M1, M2, M8, and M9 fuel loading designs. The M1 and M2 designs exhibit similar EOC core multiplication factor performances in the 0-D model, as do the M8 and M9 designs. Additionally, the M1 and M8 designs are loaded with more gadolinia than the M2 and M9 design, respectively. In consideration of gadolinia's role in controlling BOC reactivity, pairings involving the M8 and M1 fuel loading designs were given further consideration.

Table 7. LP optimization of selected fuel design pairings summary.

High Reactivity Fuel Assembly Design	Low Reactivity Fuel Assembly Design	EOC Core Effective Multiplication Factor
750M8	775M1	1.004987
750M8	795M1	1.005013
775M8	750M1	1.012312
775M8	795M1	1.011867
795M8	775M1	1.017056

Based on the LP optimization results, the selected fuel design pairing was the 795M8 and 775M1 combination. This pairing provides a sufficiently high EOC core multiplication factor to maintain criticality while achieving the desired cycle length. Additionally, it features one of the highest gadolinia loadings when compared to other evaluated pairings.

As previously discussed in Section 2.3.2, the peak exposure of an assembly did not comply with NRC burnup guidelines. Furthermore, the peak exposure reported in PARCS is a node-based value, representing the average burnup of a fuel assembly rather than the burnup of an individual fuel rod within the assembly. Rod-based power factors were utilized to obtain a more accurate estimate of maximum rod burnup for incorporation into the optimization process. Since PARCS is a nodal code, it does not directly calculate rod power factors; instead, it reconstructs rod power based on the nodal solution.

The reconstructed rod power is divided by the assembly power, where this power factor, P, is multiplied by the ratio of heavy metal loading, G, in the rod compared to the assembly, which reduces to the number of fuel rods. This produces a coefficient applied to the change in burnup, BU, from the previous depletion step to the current step. This value is then added to the previous rod burnup and accumulates over successive depletion steps. The maximum rod burnup calculation assumes an initially flat burnup distribution within the assembly, meaning it does not account for the prior burnup history of specific rod locations.

$$BU_{rod,i} = BU_{rod,i-1} + \frac{P_{rod,i} \cdot G_{assembly}}{P_{assembly} \cdot G_{rod,i}} \cdot \left(BU_{assembly,i} - Bu_{assembly,i-1}\right) \quad (1)$$

The EPUs were optimized using the selected fuel assembly designs carried out within the MIDAS framework. The constraints considered included safety and performance metrics such as peaking factors, boron concentration, max rod burnup (RBU), and cycle length (EFPD), as summarized in Table 8. The safety metrics were derived from the current plant design, while the performance metrics reflected the objectives of the extended power uprate [15].

Table 8. Objective function parameters matrix for optimization.

Constraints	Weight	Limit
Cycle Length (EFPD)	1.0	530
F_q	250	2.55
$F_{\Delta H}$	300	1.62
Boron Concentration (ppm)	1.0	1800
Max Rod Burnup (GWd/MTU)	20	80

The objective function for the optimization is used to estimate the relative fitness for solution i and $fitness_i$ was formulated as a penalty function, in which failing to meet a constraint resulted in a penalty to the fitness value, whereas satisfying the constraint resulted in no penalty or reward. The objective function considered weights (W) for each constraint to place greater emphasis on meeting the max rod burnup limit, based on the equation below. To further support compliance with the burnup requirement, the cycle length was reduced to an 18-month cycle. Ensuring this cycle length requires the cycle length constraint to match the target value, where any deviation from the target imposed a penalty on the fitness value. With the reduction in cycle length, an alternate case was developed using a feed region size of 68, under the assumption that shorter cycles require less fuel loading.

$$fitness_i = EFPD_i + W_{Boron} \cdot min(0, Boron_{limit} - Boron_i) + W_{F_q} \cdot min\left(0, F_{q\,limit} - F_{q\,i}\right) + W_{F_{\Delta H}} \cdot min\left(0, F_{\Delta H\,limit} - F_{\Delta H\,i}\right) + W_{RBU} \cdot min(0, RBU_{limit} - RBU_i) \quad (2)$$

Each optimization case evaluated a population of 280 individuals (designs) over 60 generations, resulting in a total of 16,800 designs assessed. The two cases, one with a feed region size of 84 and the other with 68, produced cycle length distributions that deviated from the target, where the mean cycle length of all designs did not meet the target or fell within one standard deviation of it. As seen in Figure 7, a lesser number of designs met the cycle length limit in the case with a feed region size of 68, where less than a majority of designs met the cycle length limit. In the case of a feed region size of 84, most of the designs met the limit, but still far exceeded the cycle length target, where a majority of the simulated designs met the limit, shown in Figure 8. This demonstrates the effectiveness of the objective function, where meeting the cycle length target constraint could be improved by an increase in weighting for the cycle length penalty.

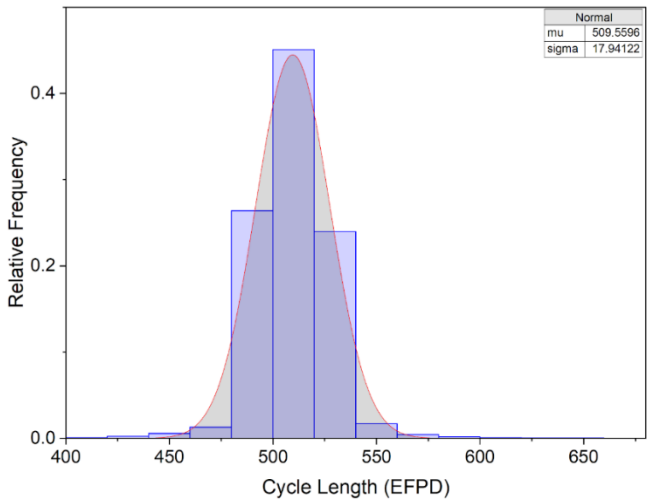

Figure 7. Distribution of cycle length among the 68-feed region size case.

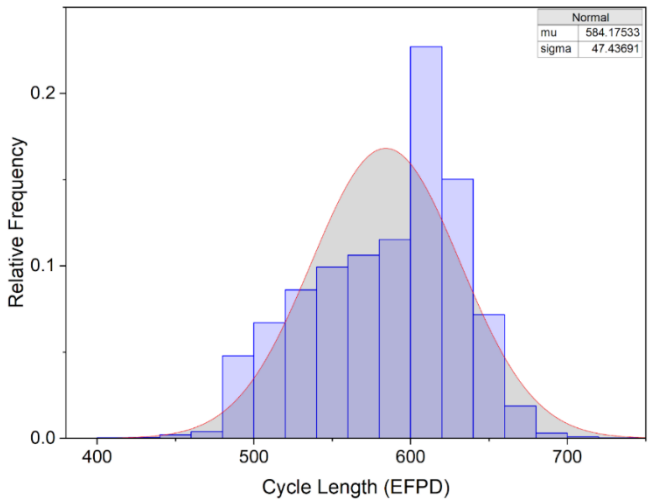

Figure 8. Distribution of cycle length among the 84-feed region size case.

A similar analysis was conducted on the optimization's ability to satisfy the max rod burnup constraint. The population of designs in the 68-feed region size case had a mean max rod burnup of 78.9 (GWd/MTU), which was below the target, with more than 50% of the designs satisfying the constraint. The mean maximum rod burnup across the population of designs was higher in the 84-feed region size case at a value of 86.9 (GWd/MTU), thus exceeding the limit where more than 50% of the designs failed to meet the constraint.

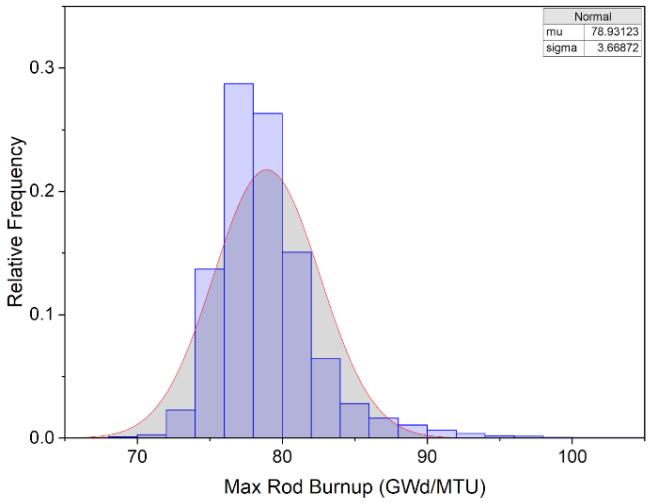

Figure 9. Distribution of max rod burnup among the 68-feed region size case.

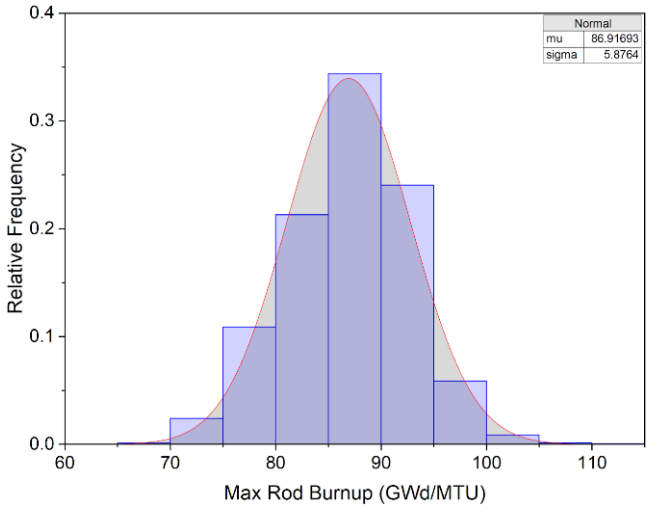

Figure 10. Distribution of max rod burnup among the 84-feed region size case.

Upon further evaluation of the 33,600 designs across the two optimization cases, no design was found to meet all specified constraints. None of the designs satisfied the $F_{\Delta H}$ constraint. Consequently, the selection of the best design was based on identifying the configuration with the lowest $F_{\Delta H}$ value while still meeting all other constraints. The resulting design complied with every constraint except $F_{\Delta H}$, where its value exceeded the limit by 9%.

Table 9. STP model optimized solution performance summary.

Objective	Value	Limit
Max. Cycle Length (EFPD)	537.49	530.00
Max. Soluble Boron (ppm)	1488.6	1800.0
EOC Max Rod Burnup (GWd/MTU)	79.66	80.00
F_q	2.399	2.550
$F_{\Delta H}$	1.795	1.650

The associated loading pattern and shuffling scheme consists of three regions. The feed region contains 68 fuel assemblies, with eight assemblies of the 795M8 design and 60 assemblies of the 775M1 design, as displayed by the quarter-core symmetry of the loading pattern and shuffling scheme in Figure 11. The twice-burned region also contains 68 fuel assemblies, while the thrice-burned region includes 57 fuel assemblies. One important note is the placement of thrice-burned fuel assemblies along the periphery. This placement might not be optimal when trying to reduce pin power peaking values.

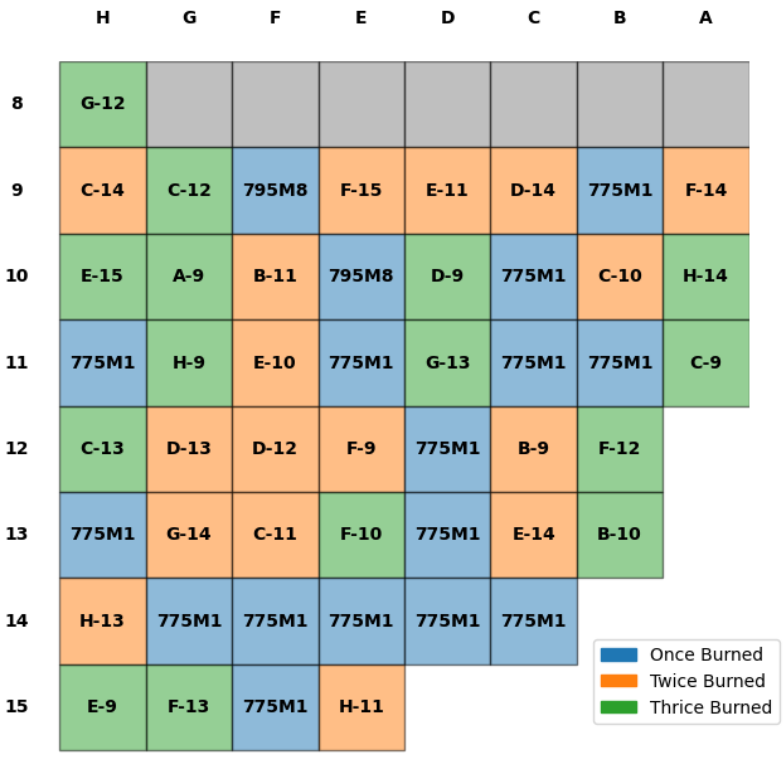

Figure 11. STP model core loading pattern and shuffling scheme.

The resulting design was further analyzed to determine the timing and location at which the maximum $F_{\Delta H}$ value occurs. The peak value is observed during the third depletion step, or on the second day of the cycle length, in fuel assembly K-11, as observed in Figure 12. By referencing the loading pattern depicted in Figure 11, the fuel assembly experiencing this peak is observed to be a fresh assembly of the 775M1 design. As previously mentioned, the thrice-burned fuel assemblies along the periphery show minimal pin power factors, in which their contribution to the core power output is very low compared to the rest of the core, hence the peaking toward the middle in a fresh assembly.

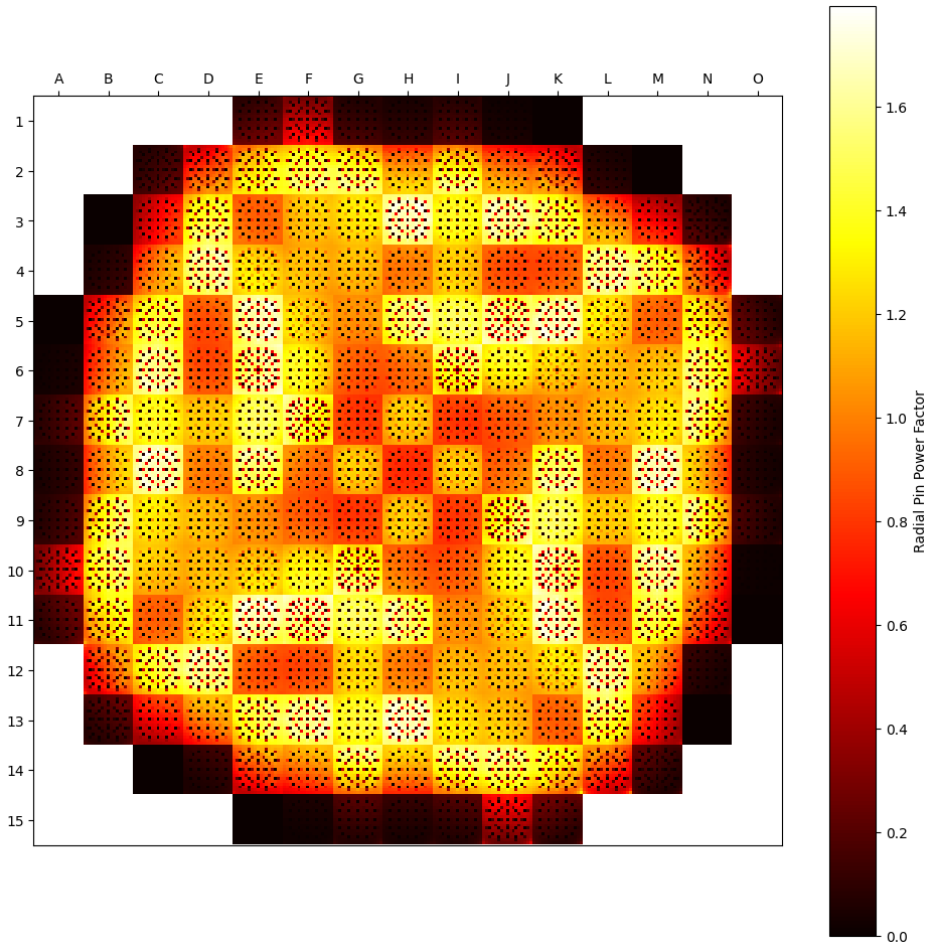

Figure 12. Radial pin power distribution of STP model at depletion step 3, 2 days into the cycle.

A closer examination of the assembly in question, presented in Figure 13, reveals noticeable peaking in the upper-left quadrant of the fuel assembly, which faces the core center. Furthermore, the fuel rods exhibiting lower peaking correspond to the gadolinia-bearing fuel rods.

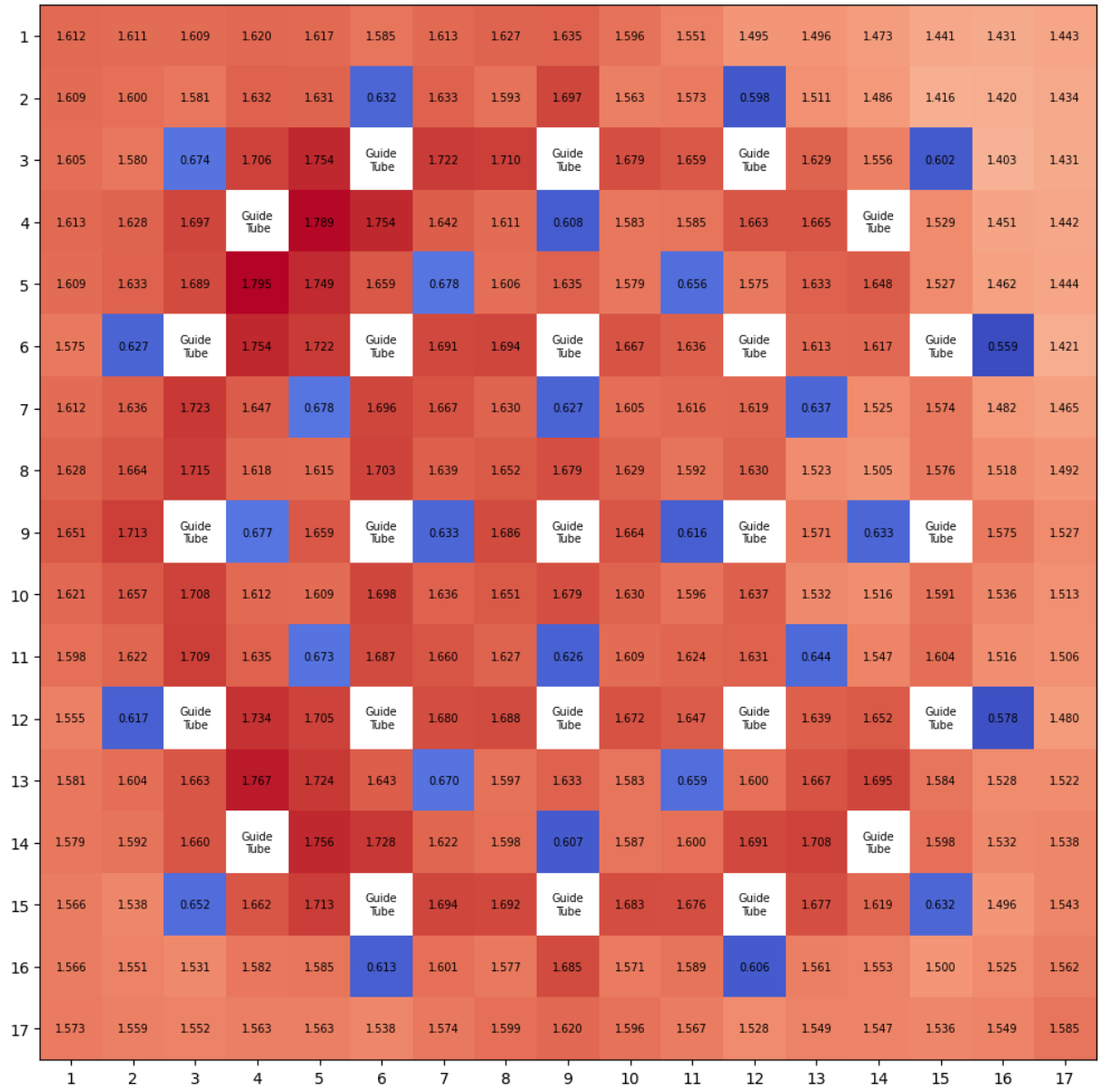

Figure 13. Radial pin power factor distribution at depletion step 3 for fuel assembly K-11 in Figure 12.

The implication of this analysis is that there must be an iterative process between fuel assembly design and core design. To minimize power peaking in the core, it must first be minimized in the fuel assembly layout, where an optimization of the fuel lattice design used to reduce power peaking will aid in reducing power peaking factors in the core simulation. In addition, the peaking in the fuel assembly is heavily influenced by its position in the core, as indicated by the pin power factor distribution in Figure 13. A potential solution to flattening the power distribution within a fuel assembly is to purposefully design fuel assemblies based on their expected placement. For example, loading a fuel assembly expected to be on the periphery to improve power influences from the edge of the core, which was lacking in this design at the BOC. A reduction in the power peaking could also reduce the max rod burnup, which was a problem described in previous sections. Including rotational motions in the shuffling scheme could also help to address this concern. For example, rotating the assembly above would expose various parts of the fuel assembly to the high-power peaking, which could reduce the overall max rod burnup. Admittedly, the

proposed solutions have the potential to complicate the design and subsequent optimization; however, to meet ambitious performance goals such as EPUs, the safety margins for meeting the constraints are small and any improvement of the design will be beneficial.

2.5 Core Optimization for Low Power Uprate

The inability to develop a design that satisfied the 18.42% power uprate safety constraints led to the creation of a new scenario. The performance goals were revised to a fixed 24-month cycle length with a reduced power uprate of 4100 MWth, corresponding to an 8% increase from the original power rating. Although less ambitious than the higher uprate, this scenario represents a step toward achieving extended power uprate goals. The change in performance parameters, particularly the reduced power, provides an opportunity to reconsider design choices such as fuel enrichment levels.

2.5.1 Reselection of Fuel Assembly Designs

To determine the appropriate degree of enrichment reduction in the fuel design, the 0-D model described in Section 2.4.1 was applied. Under the same linearity assumption used in the model, the EOC core multiplication factor was assumed to decrease linearly with decreasing enrichment. This linear relationship is fuel-design specific and not applied uniformly across all designs. The equations were derived from linear fits of enrichments at 7.50%, 7.75%, and 7.95%, which are shown to the right of the vertical dotted line in Figure 14. Each fuel design was evaluated at its respective EOC multiplication factor, considering a leakage probability of 6%, the suggested threshold for maintaining criticality. For a single fuel design core, the selected designs were required to meet this threshold at or below an enrichment of 7.5%. As shown in Figure 14, the M4, M8, and M9 fuel designs satisfied this criterion. Based on past optimization experience with this core model under similar goals, M8 was selected as the primary fuel design.

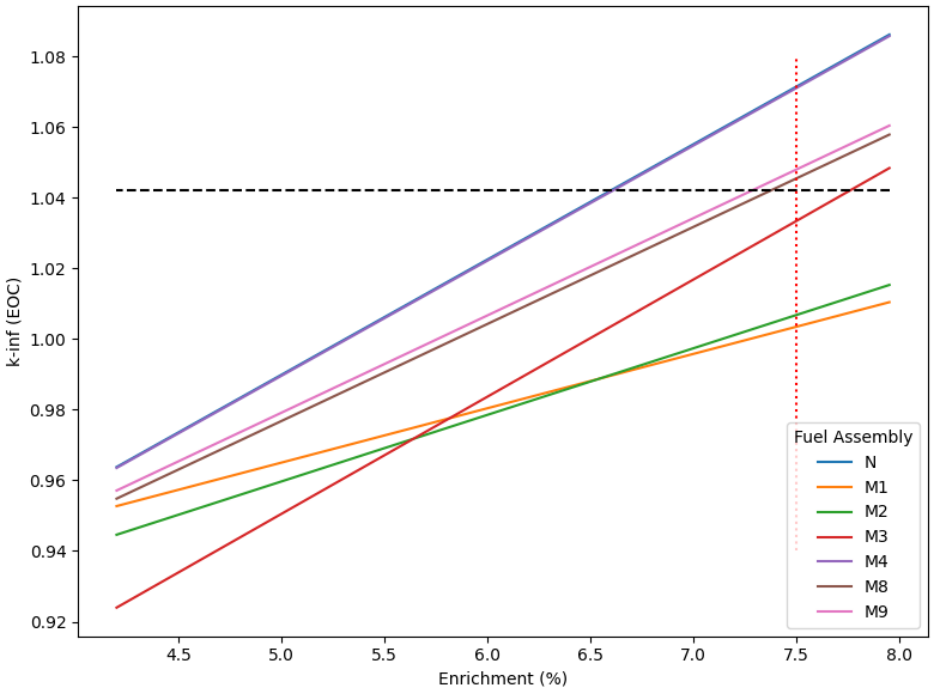

Figure 14. Predicted trend of fuel design's core EOC multiplication factor as enrichment varies.

As described in Section 2.4.1, combinations of fuel designs can be used in a core to maintain criticality over the cycle length. For a 2-fuel design core, the M3 fuel design was selected, with its

purpose being to help maintain acceptable power peaking factor values. The enrichment levels for the fuel designs were based on M8's threshold crossing at approximately 7.25%. To address inaccuracies in the 0-D model assumptions and to prioritize lower enrichment, enrichments of 7.0% and 7.25% were evaluated in the core design optimization. Reducing enrichment within the fuel rod required corresponding adjustments to gadolinia concentration. Table 10 summarizes the updated enrichments and gadolinia weight percentages.

Table 10. Reduced ^{235}U enrichment for various gadolinia concentrations and lower LEU+ enrichments.

Nominal ^{235}U Enrichment	**Reduced ^{235}U enrichment**			
	Concentration of Gd_2O_3-bearing rods			
	2 w.t.%	4 w.t.%	6 w.t.%	8 w.t.%
7.50%	6.75	6.00%	5.25	4.50%
7.25%	6.53	6.20%	5.08	4.65%
7.00%	6.30	6.36%	4.90	4.77%

2.5.2 Extended Low Power Uprate Optimization Strategy and Parameters

The objective function considerations were similar to those used in the high power uprate optimization, with the same safety constraints and performance goals applied. To emphasize compliance with the $F_{\Delta H}$ constraint, the objective function was weighted to heavily penalize the fitness value if the limit was exceeded, as shown in Table 11. In addition, the maximum allowable feed region size for placing fresh fuel assemblies was set to 88. The purpose of this increased feed region was to load the core with sufficient fresh fuel to reduce the maximum rod burnup within fuel assemblies.

Table 11. Updated optimization parameters for low power uprate scenario.

Constraints	**Weight**	**Limit**
Cycle Length (EFPD)	1.0	700
F_q	250	2.55
$F_{\Delta H}$	500	1.62
Boron Concentration (ppm)	1.0	1800
Max Rod Burnup (GWd/MTU)	20	80

A few optimization cases were developed based on enrichment level and the type of fuel designs included. Some cases prioritized a single fuel design core at 7.0% and 7.25% enrichments. Reducing the number of fuel designs to one simplified the design and decision space for the optimizer, making the solution space more manageable and improving the potential to exploit good solutions. In addition to the single fuel design cases, a two-fuel design core using the M8 and M3 designs was evaluated. The enrichment level for these designs was set to 7.0%, with the feed region size considered sufficient for the two-fuel design core to meet the target cycle length.

2.5.3 Results of Extended Low Power Uprate Optimization

The initial optimization cases with single fuel design cores at 7.0% and 7.25% enrichment produced performance results similar to the high power uprate scenario. As shown in and Figure 15 and Figure 16 for the 7.0% and 7.25% cases, respectively, both exhibited a similar average cycle length across their solution populations. The key difference lies in the spread of the distributions, where the 7.0% case showed a wider spread than the 7.25% case, with some designs within one standard deviation achieving the desired cycle length.

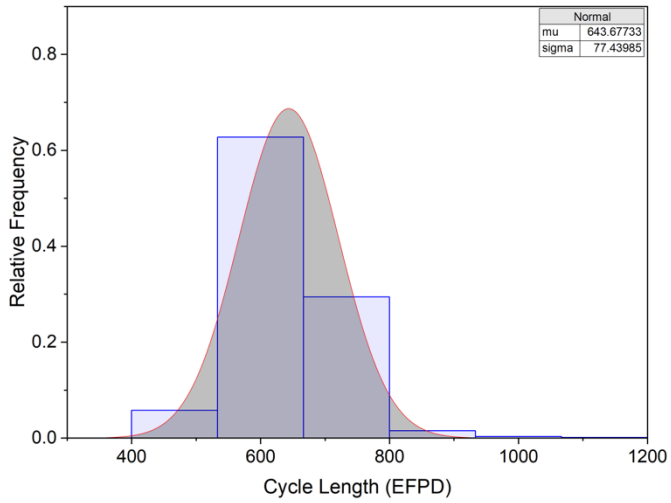

Figure 15. Distribution of cycle length for the 7.0% enriched single fuel design core.

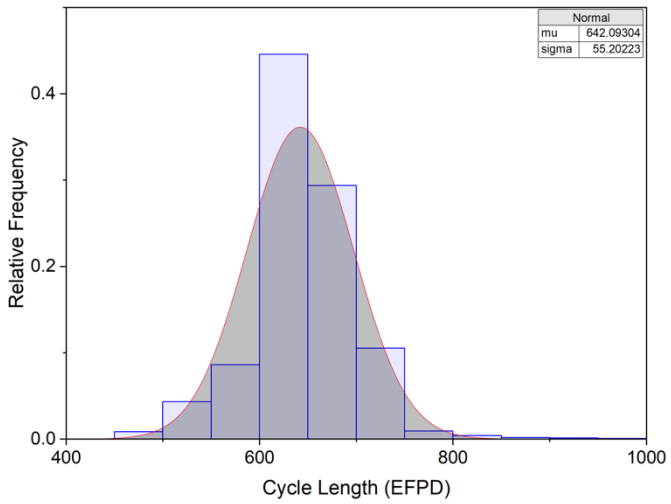

Figure 16. Distribution of cycle length for the 7.25% enriched single fuel design core.

Considering the maximum rod burnup constraint, only one design satisfied the limit. As shown in and Figure 17 and Figure 18, the maximum rod burnup distributions for both cases are similar, where both distributions are primarily above the constraint limit. The average values and spreads are nearly the

same at around 96 GWd/MTU ± 5 GWd/MTU, with the key distinction being that the 7.0% case produced a design at the lower extreme, which met the constraint.

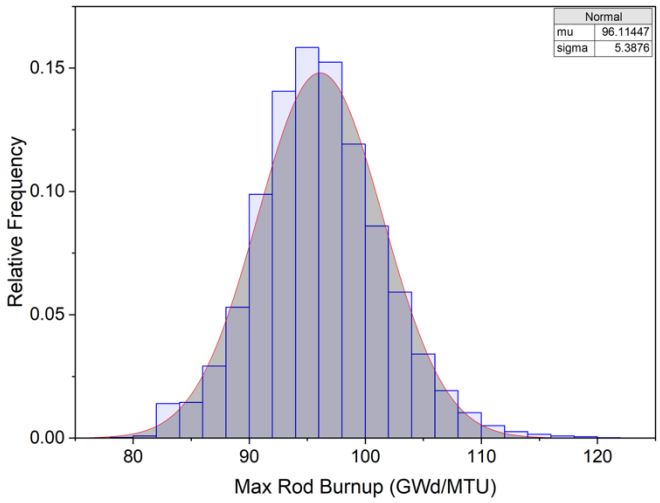

Figure 17. Distribution of max rod burnup for the 7.0% enriched single fuel design core.

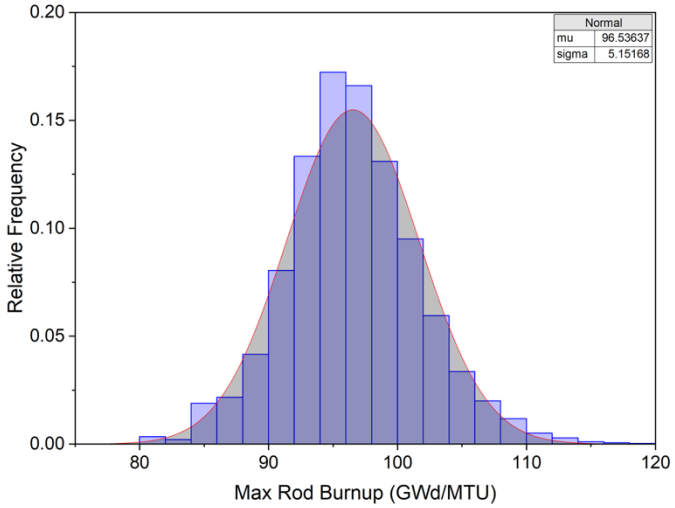

Figure 18. Distribution of max rod burnup for the 7.25% enriched single fuel design core.

Focusing on the design from the 7.0% case that met the maximum rod burnup limit, Table 12 shows that the design satisfied all constraints except for the $F_{\Delta H}$ value. The cycle length of this design exceeds the target by 30 EFPD, which is acceptable for meeting the desired cycle length but may be too long for practical operation. Regarding margins between results and their respective limits, F_q and maximum rod burnup have smaller margins compared to maximum soluble boron.

Table 12. Summary of results from the best solution in the 7.0% case.

Objective	Value	Limit
Max. Cycle Length (EFPD)	730.726	700.00
Max. Soluble Boron (ppm)	1461.3	1800.0
EOC Max Rod Burnup (GWd/MTU)	78.58	80.00
F_q	2.527	2.550
$F_{\Delta H}$	1.873	1.650

Examining the $F_{\Delta H}$ or similarly described as the radial pin power factor (RPF), distribution within the core, the peak RPF occurs in assembly G-4, as shown in Figure 19. The RPF distribution is relatively flat at the core center. Moving outward, assemblies in the middle radius exhibit noticeable power peaking, while those near the edge contribute little to the core power. Within the middle-radius region, slight dips or peaks in RPF correspond to the assemblies' burnup stages. For example, F-5 exhibits a flatter RPF distribution than G-4, despite their similar radial locations, with F-5 being closer to the core center. Surrounding assemblies influence each assembly's RPF, but the primary difference is that G-4 is a fresh assembly, whereas F-5 has been burned twice in the equilibrium cycle. Because fresh assemblies have higher reactivity during initial burnup stages, the observed peaking in G-4 at BOC is expected.

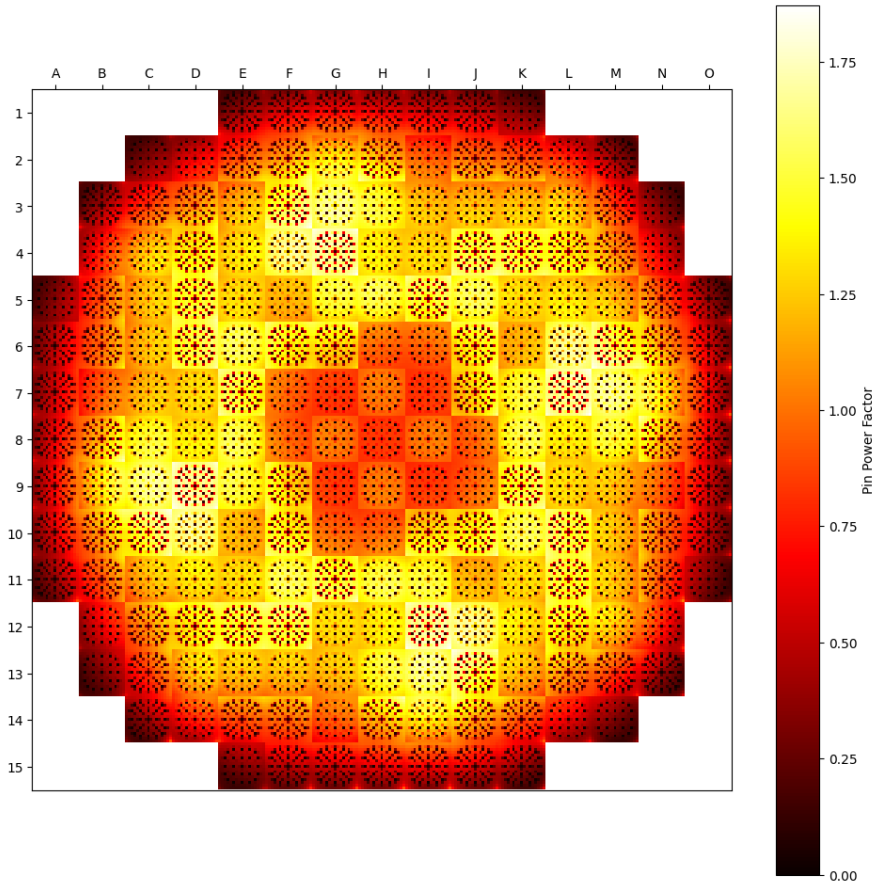

Figure 19. Radial pin power factor distribution for core design in 7.0% case at BOC.

The peak RPF within the core occurs in assembly G-4, specifically in the lower-right quadrant corner fuel pin, as shown in Figure 20. Among the assembly's fuel pins, this pin is one of the closest to the core center and is surrounded by once-burned fuel assemblies. Figure 20 shows that the RPF increases toward the corners and decreases in the gadolinia-bearing fuel pins. The pronounced dips in RPF within the gadolinia-bearing pins highlight gadolinia's effectiveness in controlling initial reactivity.

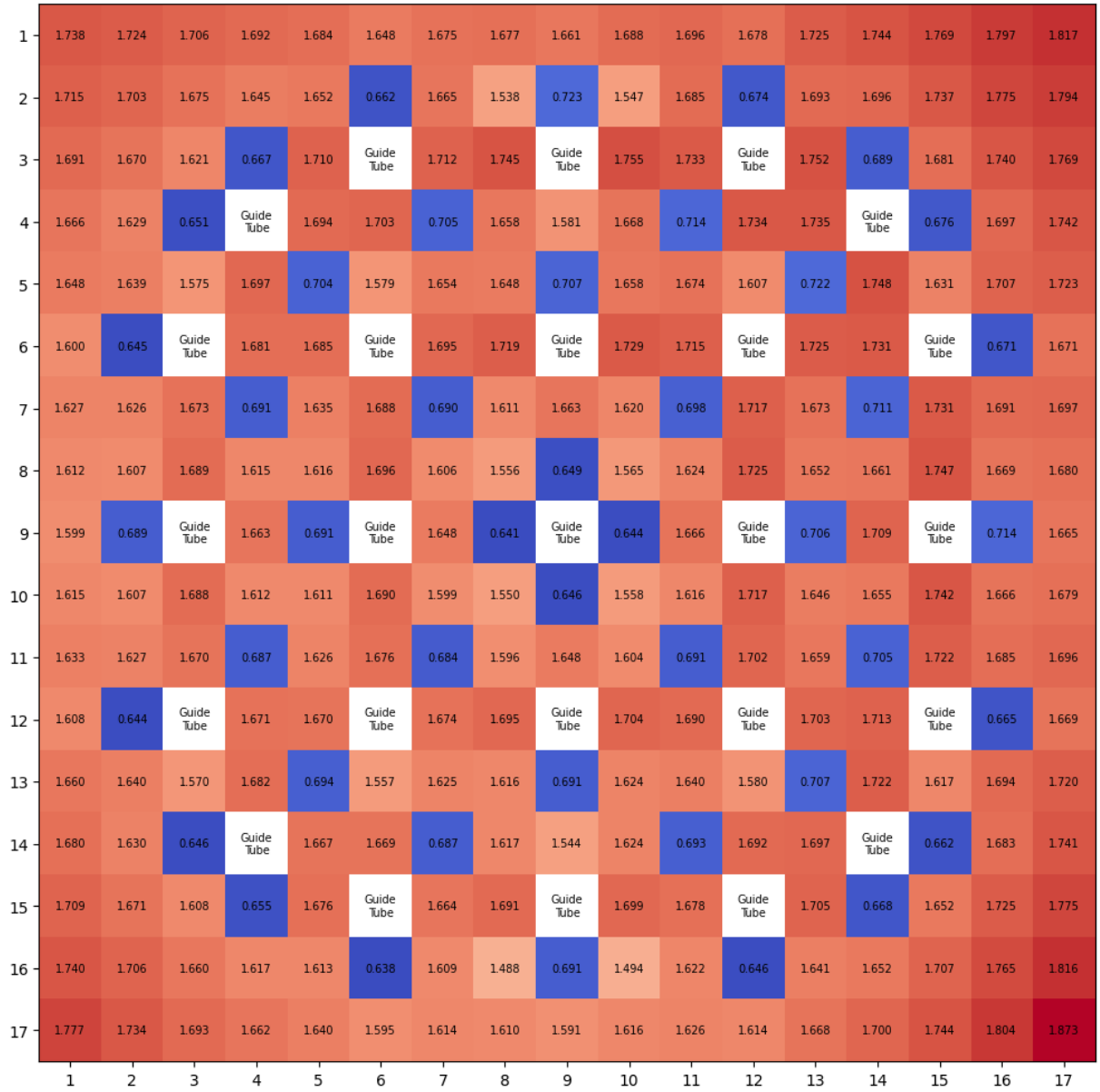

Figure 20. Radial pin power factor distribution within the G-4 assembly of the core simulation at BOC.

Comparing Figure 19 with Figure 12 from the high power uprate scenario highlights differences in power contributions from the core periphery, primarily due to the placement of once- and thrice burned fuel assemblies. Figure 11 shows much of the periphery consists of thrice burned assemblies, whereas Figure 21 shows that most assemblies in this region are once-burned or fresh. Beyond influencing power distribution, this also affects leakage. Compared to the selected designs from the high power uprate

scenario, this design exhibits a leakage of 4.71%, aligning more closely with the conservative estimate from the 0-D model. While this relates to the impact on the reactor pressure vessel, vessel fluence was not considered in this study.

Figure 21. STP quarter-core loading pattern and shuffling scheme for selected design from 7.0% case.

The two-fuel design core optimization case produced maximum rod burnup and cycle length distributions similar to the initial single fuel design core cases. The best solution from this optimization did not outperform the single fuel design solution, with the maximum rod burnup constraint exceeded by 4.5 GWd/MTU. Although the additional fuel design yielded a more desirable $F_{\Delta H}$ value, it was insufficient to meet the constraint. There was no evidence that the additional fuel assembly improved the overall solution population. In the best solution, the peak RPF occurred in the M3 design near the middle of assembly C-4, as shown in Figure 22.

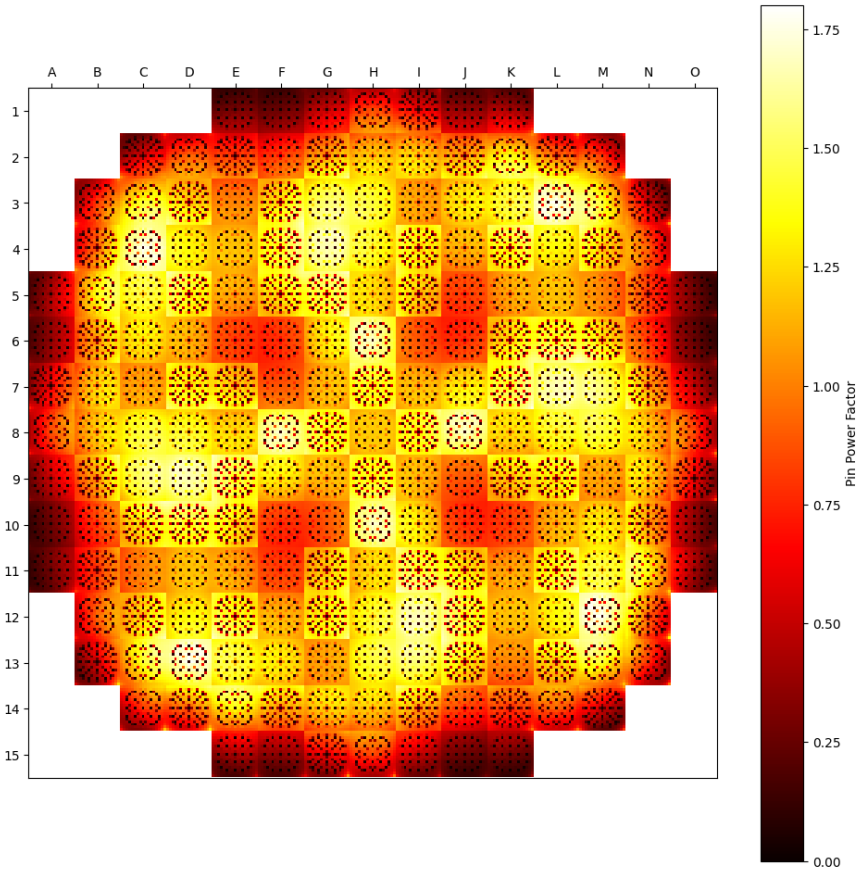

Figure 22. Radial pin power factor distribution for two-fuel design core case in low power uprate scenario at BOC.

2.5.4 Proposed Actions

The results of the extended low power and high-power optimizations are similar in that the best solutions met all constraints except for $F_{\Delta H}$. Both scenarios also exhibited similar maximum rod burnup distributions, with the majority of designs in the solution populations being unsatisfactory. What follows is a series of proposed actions to address the inadequacies of the optimization case's results and subsequent designs. The results from the extended low power uprate scenario are the basis for the suggestions but apply to power uprate scenarios in general, including the high power uprate scenario.

The most persistent issue observed in the core design optimization was maintaining the $F_{\Delta H}$ limit. Across all optimization cases and scenarios, no design satisfied this constraint. With the constraint being pin based, the fuel design was further evaluated. As the $F_{\Delta H}$ calculation in PARCS is based on pin power factors from the fuel design simulation software POLARIS, the pin power factor values at the initial reference state were examined for the M8 and M3 designs. Comparing Figure 23 with Figure 24 shows that M8 has higher pin power peaking factor values than M3. Furthermore, the gadolinia bearing fuel pins with 2 w.t. %, with RPF values of 0.48, showed to have a less extreme RPF than the larger w.t. % fuel pins. Additionally, M8 peaks occur in the corners, while M3 peaks occur near the center. This aligns with core simulation observations, where the peak $F_{\Delta H}$ occurred either at the corner of M8 assemblies or toward the center of M3 assemblies, indicating that pin-level peaking directly influences core-level peaking.

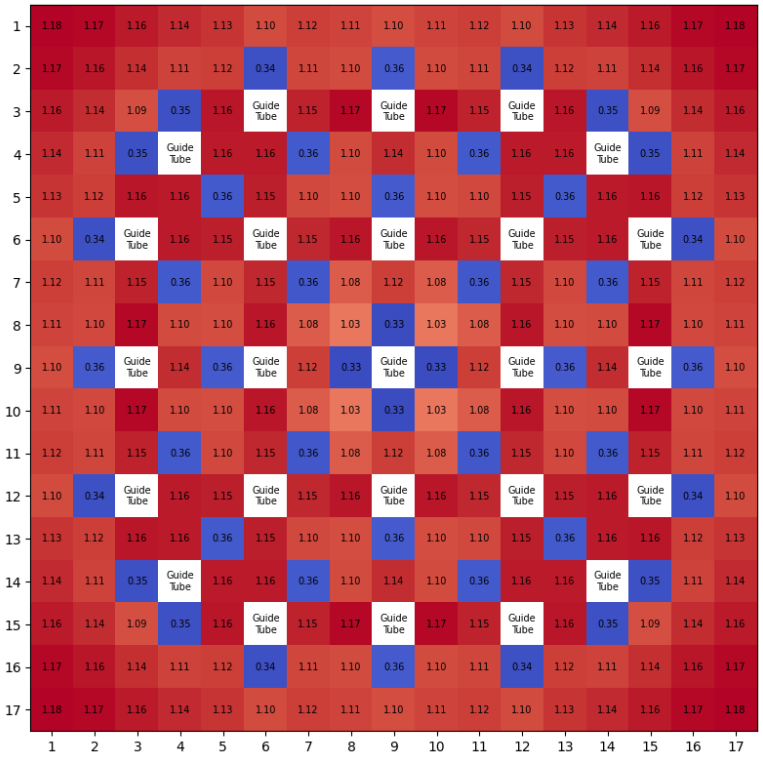

Figure 23. Radial pin power factor distribution at a given reference state for the M8 fuel design.

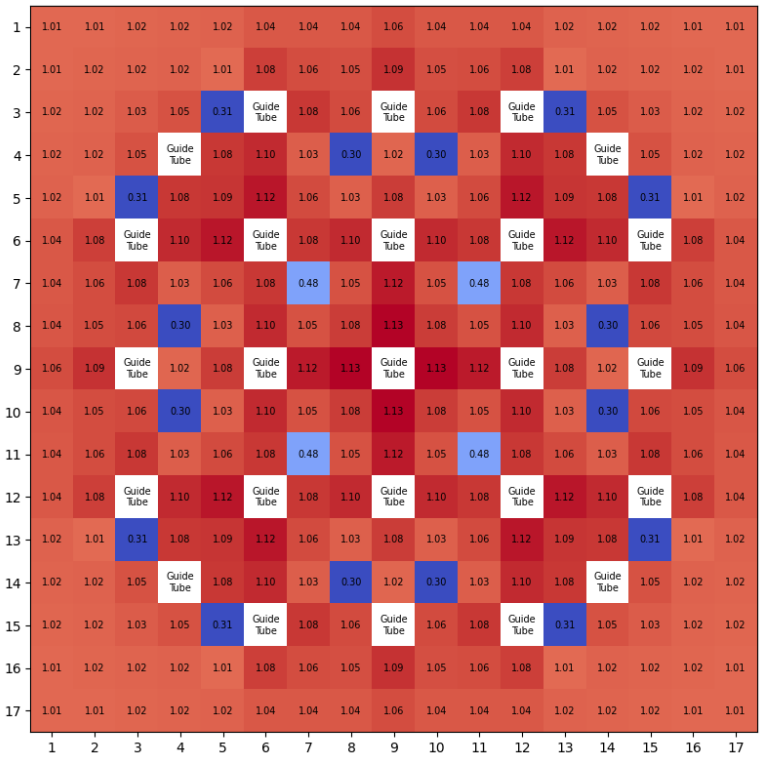

Figure 24. Radial pin power factor distribution at a given reference state for the M3 fuel design.

Another consideration is the timing of RPF peaking. The peaking pins in the M8 and M3 designs were observed to originate from fresh assemblies, typically near the start of the cycle. Tracking the progression of peak RPF over assembly burnup, as shown in Figure 25, both fuel designs start with relatively high values. As the fresh assembly and gadolinia are depleted, the peak RPF decreases, eventually declining gradually with increasing burnup. Regarding assembly enrichment, increasing enrichment affects the RPF over burnup, but not significantly. As seen in Figure 25 between the 7.0% M8 and 7.95% M8 fuel designs, as well as between the 4.20% IFBA-128 and 4.60% IFBA-128 fuel designs, the burnable absorber-loading pattern is the same, but the enrichments differ, respectively. Similar fuel designs with different enrichments begin at comparable RPF values but follow slightly different trends, indicating that the burnable absorber pattern of the fuel design itself has a more substantial impact on peak RPF than enrichment level.

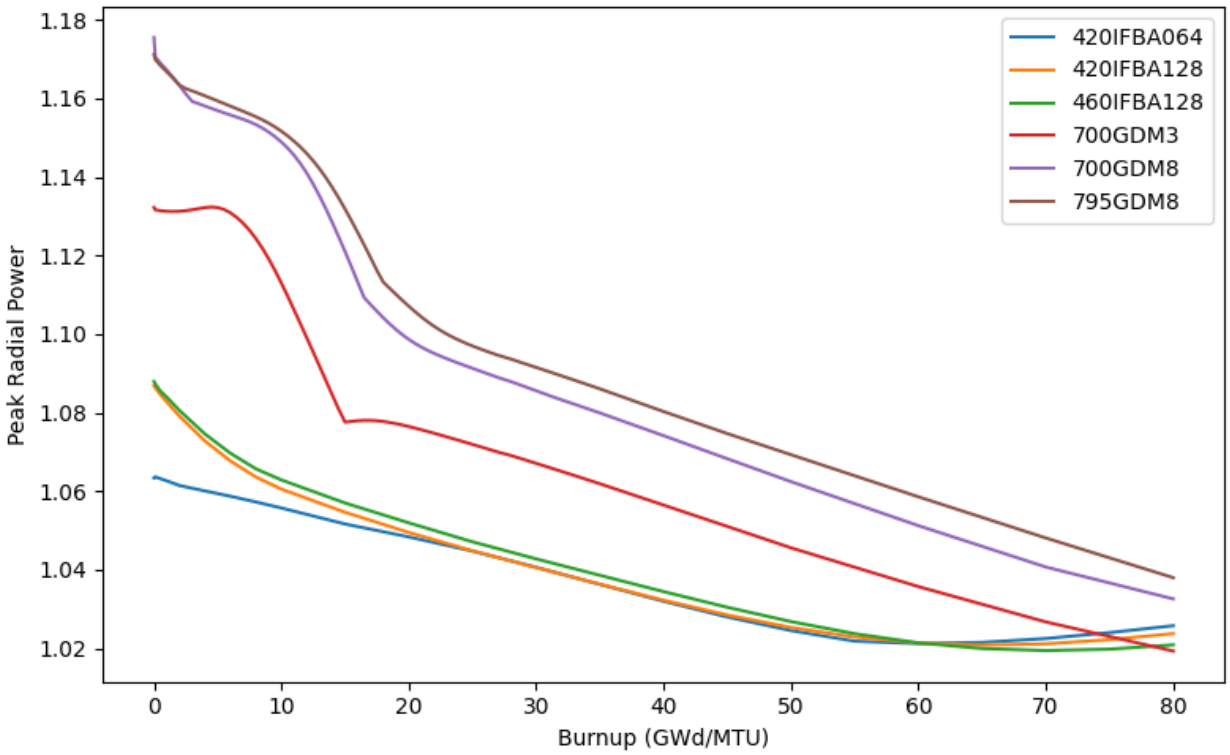

Figure 25. Progression of fuel design's peak radial pin power factor as burnup increases.

Comparing different burnable absorbers, such as IFBA and gadolinia, both produced the expected effects, with gadolinia better controlling initial excess reactivity. The drawback is its influence on RPF. As shown in Figure 25, IFBA fuel designs start with lower peak RPF than gadolinia designs. This is largely due to gadolinia's effectiveness in controlling excess reactivity and creating neutron sinks, as evident in the power distributions for the M3 and M8 fuel designs. With fuel design RPF normalized to one, the distribution of individual pin powers was examined. Comparing the RPF distributions of the M8 and IFBA128 designs, shown in Figure 26 and Figure 27 respectively, the IFBA design exhibits a tighter distribution, while the M8 design displays a more bimodal distribution.

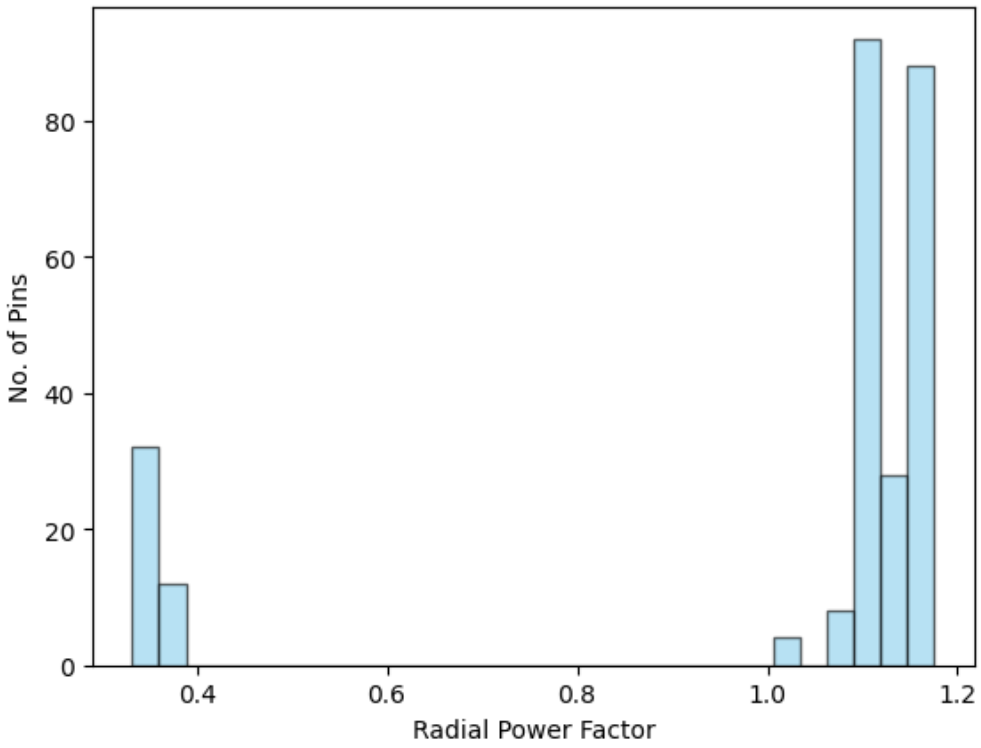

Figure 26. Radial pin power factor distribution amongst the fuel pins within the 7.0% M8 fuel design.

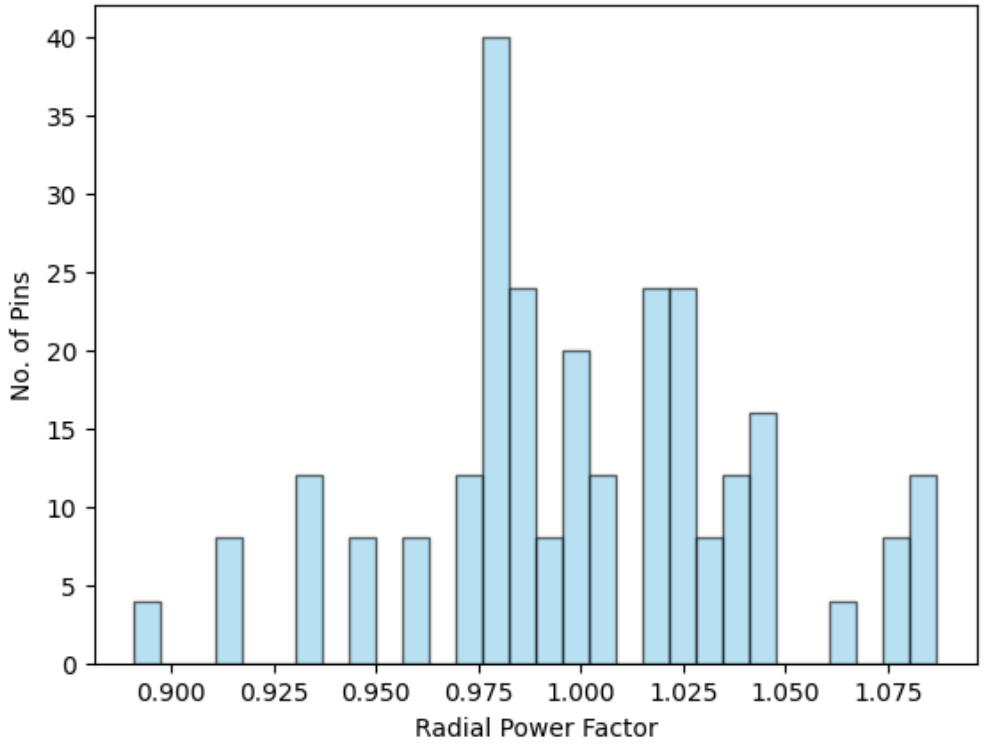

Figure 27. Radial pin power factor distribution amongst the fuel pins within the 420IFBA128 fuel design.

The disparity between fuel design RPF distributions indicates that gadolinia-based designs exhibit more significant extremes, while IFBA designs are more centralized. Since the RPF are normalized to one, as one extreme moves further from the mean, the opposite extreme likely shifts as well, as seen in Figure 26. The RPF distributions and the progression of peak RPF demonstrate that IFBA designs better manage the $F_{\Delta H}$ value, whereas gadolinia designs more effectively control initial reactivity and maximum boron concentration. To leverage the strengths of both burnable absorbers, fuel designs incorporating both IFBA and gadolinia rods could be beneficial.

Additionally, reducing the gadolinia weight percentage in the fuel rods while maintaining the same, or at a reduced, assembly loading can help mitigate extremes, as seen in the M3 and M8 RPF distributions. The max boron concentration margin allows for such a reduction in gadolinia loading without compromising the specified limit. One approach to determining the fuel lattice loading pattern is to optimize similarly to the core design, minimizing peak pin power as the objective. Alternatively, one could aim to reduce the spread of the pin power distribution by minimizing its standard deviation. For example, the standard deviation of the 4.20% enriched with 128 IFBA rods design is 0.04, compared to 0.29 for the 7.0% M8 gadolinia design. For the gadolinia-based designs, an approximate 86% reduction would achieve a standard deviation comparable to IFBA, helping both to reduce peak $F_{\Delta H}$ and maintain effective reactivity control. With this fuel design optimization, ambitious performance scenarios, such as extended power uprates, could benefit from a coupled optimization of both fuel design and core design, improving the solution population and the resulting best solution.

To address excessive maximum rod burnup, several strategies can be employed. As shown in Figure 17, the maximum rod burnup distribution for the 7.0% case exceeds the limit, with a mean of 96.1 GWd/MTU and over 99% of solutions above the limit. This indicates a need to increase enrichment, so that the fuel pins can be loaded with more fuel and therefore reduce the burnup they experience over the cycle length. While 7.0% enrichment fuel designs can maintain criticality over the cycle, the fuel is overutilized, causing the constraint to be almost always unmet.

Compared to the original goal of a 24-month cycle extension and an 18.42% power uprate, the low power uprate cycle burnup is similar but slightly lower due to reduced power. Increasing enrichment to 7.95%, as in the high power uprate study, should be investigated for the low power uprate and used as a baseline for further adjustment. This is expected to shift the maximum rod burnup distribution closer to the limit. Another potential enhancement is to impose additional restrictions on fuel batches, particularly regarding discharged fuel designs.

Table 13 shows the composition of the single fuel design best solution and the discharge distribution among regions. One of the once-burned assemblies was discharged, lowering the average discharge burnup. Ideally, all of the discharged assemblies would come from the thrice burned or twice-burned region to maximize fuel utilization in a single fuel design system. The implication is that the discharged assemblies can be placed to maximize the fuel utilization without exceeding the limit.

Table 13. Composition of discharged fuel assemblies in 7.0% case.

Region	Number of Assemblies	Average BU (GWd/MTU)	Max BU (GWd/MTU)
Thrice Burned	6	74.52	78.6
Twice Burned	15	65.31	73.1
Once Burned	1	42.2	42.2

A specific strategy to reduce maximum rod burnup and improve fuel utilization is to split the feed region in a two-fuel design system into separate batches. One batch, with lower enrichment or reactivity, is discharged solely in the twice-burned region, while a higher-enriched design is discharged in the thrice-burned region. In the low power core optimization for the two-fuel design system (M3 and M8), Table 14 shows a discharge distribution similar to the single fuel design case, with one assembly from the once-burned region and the majority from the twice-burned region.

Since M3 has higher reactivity but the same enrichment as M8, its average burnup is higher than M8 in the twice- and thrice-burned regions. An example of implementation of the suggested strategy for this system is that the higher-reactivity M3 fuel design would have greater enrichment than the lower-reactivity M8 design. The M3 design would be discharged only from the thrice-burned region, while the M8 design would be discharged solely from the twice-burned region, which is expected to improve the compliance with the maximum rod burnup constraint.

Table 14. Composition of discharged fuel assemblies in two-fuel design case.

Region	**Number of Assemblies**		**Average BU (GWd/MTU)**		**Max BU (GWd/MTU)**	
	M3	**M8**	**M3**	**M8**	**M3**	**M8**
Thrice Burned	1	5	83.3	74.8	83.3	84.3
Twice Burned	5	10	69.0	63.84	70.7	70.4
Once Burned	0	1	0	27.8	0	27.8

The lack of significant disparity in maximum rod burnup between the fuel designs indicates that a two-fuel design system with identical enrichment does not take advantage of splitting the feed region. Introducing differences in enrichment and specifying the discharge regions has a few implications. First, it reduces the average enrichment of the feed region, as high-enriched designs can be offset by lower-enriched designs.

Additionally, constraining designs to discharge from specific regions provides a buffer before fuel reaches the maximum rod burnup limit. Using lower-enriched fuel for part of the cycle and higher-enriched fuel for the full duration allows each design to be fully utilized without exceeding safety constraints. Ultimately, combining increased enrichment with batch constraints offers a better chance for an optimization case to identify several design solutions that satisfy the maximum rod burnup constraint.

3. RELAP5-3D ANALYSIS

3.1 Thermal hydraulic modeling

A RELAP5-3D model of the STP NPP was used for performing the steady-state and transient analysis using the new core configurations [3, 16]. The RELAP5-3D STP model is composed of:

1. The reactor pressure vessel, including the downcomer, downcomer bypass, lower plenum, fuel assemblies, upper plenum, and the upper head. Leakage paths are also represented: downcomer to upper plenum, cold leg inlet annulus to upper plenum, and upper plenum to the upper head by way of the guide tubes.
2. Reactor coolant system, which consists of the four primary coolant loops each containing a hot leg, U-tube steam generator, pump suction leg, pump, and cold leg. The pressurizer was attached to the C-loop, and the pressurizer spray lines were attached to the cold leg.
3. Partial balance of plant, which includes steam generator, downcomer, boiler region, separator and dryer region, and the steam dome. The major flow paths of the steam line out to the turbine governor valves are modeled. Each line from the steam generator secondary out to the common steam header is modeled individually, and includes a main steam line isolation valve, a check valve, safety relief valves, and power-operated relief valves.
4. Feedwater system, which includes the main feedwater system and the auxiliary feedwater system. The control system models include a steam dump control system, steam generator level control, pressurizer pressure control system, and pressurizer level control systems, etc.
5. Emergency core cooling system, which includes low-pressure injection (LPI) and high-pressure injection (HPI).

The reactor core model resolution has been increased compared to the model described in the previous study [16]. While the previous model grouped the core assemblies into six concentric hydrodynamic elements, the current model uses 194 RELAP5-3D “pipe” components, allowing the thermal-hydraulic modeling of 193 individual fuel assembly. The 194th “pipe” component models the volumes of the radial reflector. Each “pipe” has an associated heat structure which models the 264 fuel pins of the single fuel assembly or the stainless-steel material of the radial reflector. Thus, the new core model uses 194 heat structures. Modeling each fuel assembly independently allows an easy coupling with the neutronic core simulator and an immediate execution of non-symmetric transient analyses, like the rod ejection accident (REA). The following Figure represents the core mapping of the thermal-hydraulic components of the RELAP5-3D model.

	A	B	C	D	E	F	G	H	J	K	M	N	P	Q	R	S	T
1					943	943	943	943	943	943	943	943	943				
2			943	943	943	750	751	752	753	754	755	756	943	943	943		
3		943	943	757	758	759	760	761	762	763	764	765	766	767	943	943	
4		943	768	769	770	771	772	773	774	775	776	777	778	779	780	943	
5	943	943	781	782	783	784	785	786	787	788	789	790	791	792	793	943	943
6	943	794	795	796	797	798	799	800	801	802	803	804	805	806	807	808	943
7	943	809	810	811	812	813	814	815	816	817	818	819	820	821	822	823	943
8	943	824	825	826	827	828	829	830	831	832	833	834	835	836	837	838	943
9	943	839	840	841	842	843	844	845	846	847	848	849	850	851	852	853	943
10	943	854	855	856	857	858	859	860	861	862	863	864	865	866	867	868	943
11	943	869	870	871	872	873	874	875	876	877	878	879	880	881	882	883	943
12	943	884	885	886	887	888	889	890	891	892	893	894	895	896	897	898	943
13	943	943	899	900	901	902	903	904	905	906	907	908	909	910	911	943	943
14		943	912	913	914	915	916	917	918	919	920	921	922	923	924	943	
15		943	943	925	926	927	928	929	930	931	932	933	934	935	943	943	
16			943	943	943	936	937	938	939	940	941	942	943	943	943		
17					943	943	943	943	943	943	943	943	943				

Figure 28. Hydrodynamic model of the reactor core; “Pipe” and heat structure components numbering.

The core neutronics were simulated using the Nodal Eigenvalue, Steady-state, Transient, Le core Evaluator (NESTLE) code [6], which is embedded as an internal routine within RELAP5-3D. The NESTLE-based routine is able to model the reactor core using Cartesian and hexagonal geometries. It works by solving few-group neutron diffusion equations, where two groups are used in this project. It has several cross-section modeling options including Xenon and Samarium effects. NESTLE uses a nested non-linear iterative solution strategy that requires thermal-hydraulic feedback [6].

The cross-section database for specific fuel temperature, coolant temperature, coolant density, fuel burnup, and boron density was obtained from POLARIS. This database was then interpolated for the fuel and coolant conditions in RELAP5-3D, and the variation coefficients were also calculated. This method allows NESTLE and RELAP5-3D to perform transient calculations and update the fuel’s cross sections to estimate reactor power accordingly.

As a verification activity, after the implementation of the main cross section database in RELAP5-3D, the main fuel cycle parameters were derived (e.g., Figure 29 shows the statistics of fuel burnup for each 193 fuel assemblies at the EOC condition). As expected, the burnup is skewed toward the bottom section of the core. An HFP steady-state condition was simulated in RELAP5-3D before analyzing transient scenarios. RELAP5-3D core axial power distributions were compared with PARCS axial power

distributions, as shown in Figure 30. The Figure shows that there is an excellent agreement between the two codes. Deviation between the k_{eff} was in the order of ~40 pcm. Note that they are generally not expected to produce the exact same results because they have different levels of fidelities and different numerical kernels [3, 6, 13].

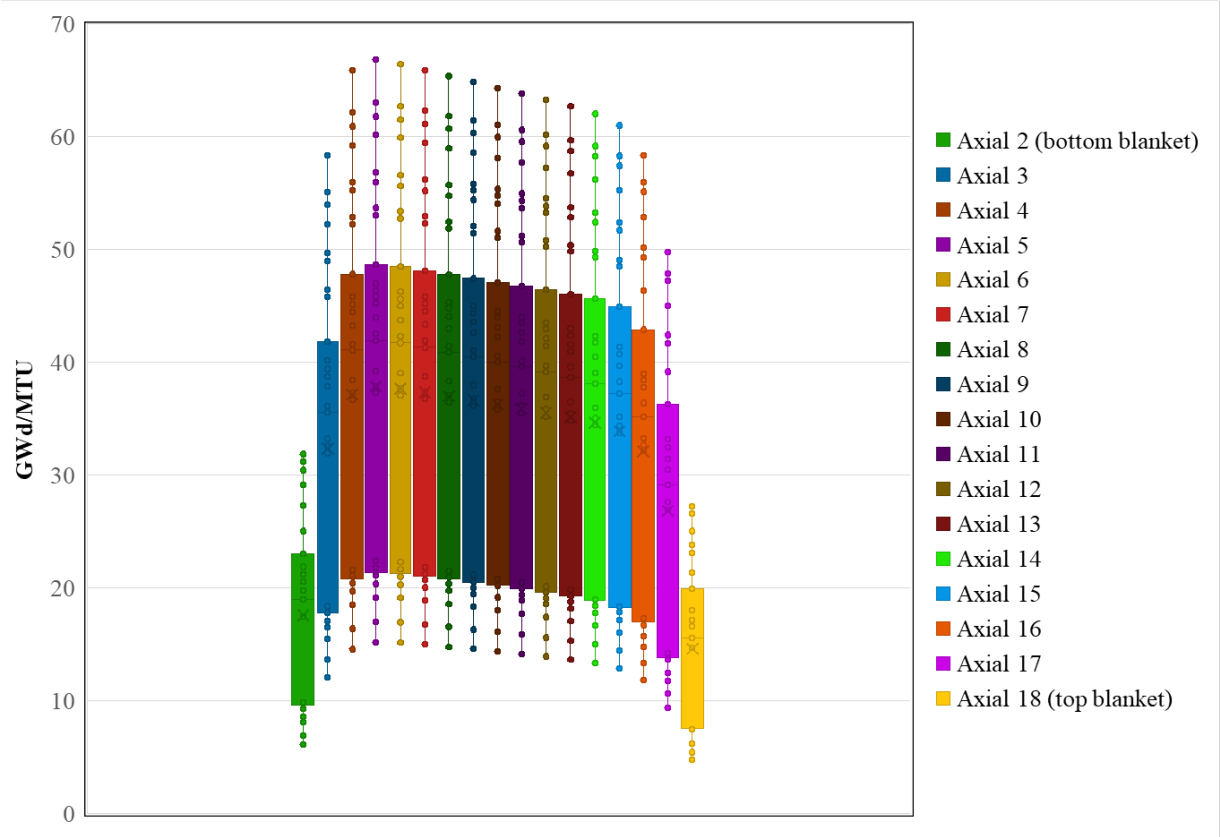

Figure 29. Box and Whisker plot showing the end-of-cycle fuel burnup distribution across RELAP5-3D axial mesh segments #2 through #18.

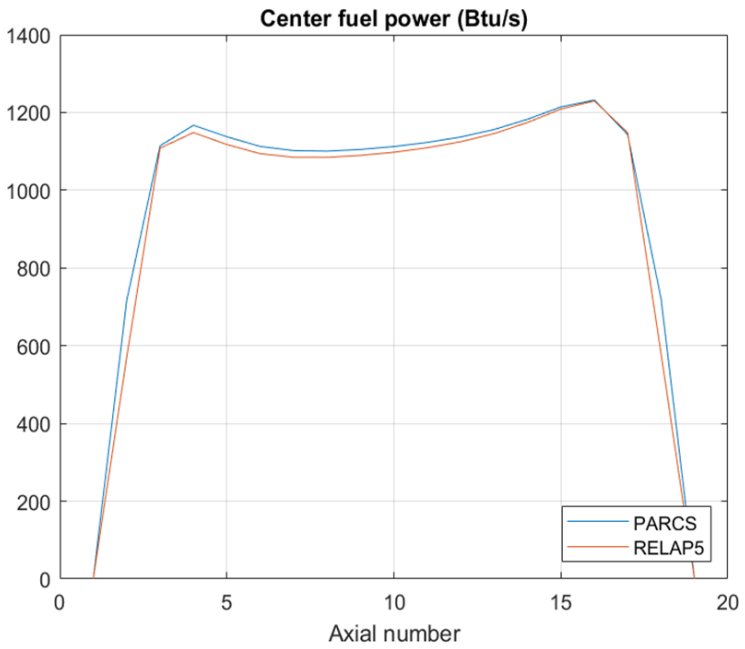

(a) Center fuel comparison

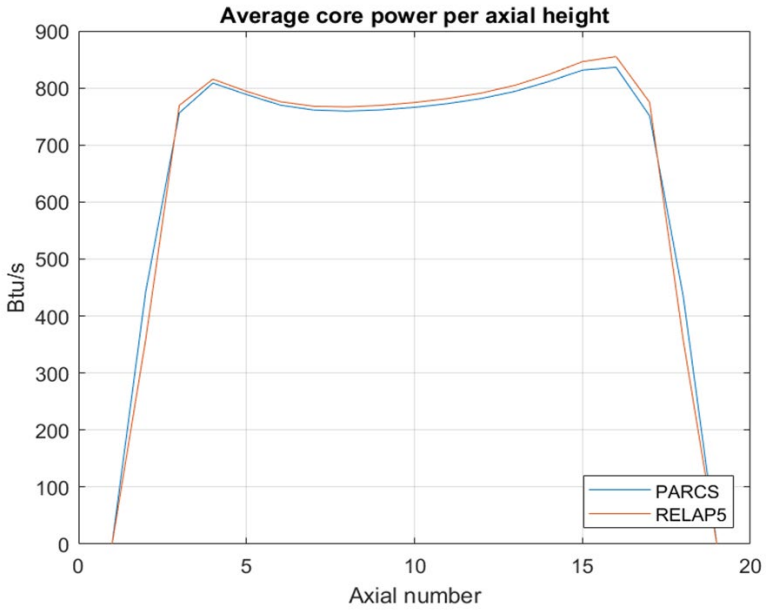

(b) Core-averaged comparison

Figure 30. Core power comparison between RELAP5-3D and PARCS at EOC.

Steady-state results from RELAP5-3D were used to calculate hot channel factors, which are important safety metrics including:

- Radial peaking factor at elevation Z, calculated as:

$$F_{(xy)}(Z) = \frac{maximum\ power\ density\ at\ elevation\ Z}{average\ power\ at\ elevation\ Z} \quad (13)$$

- Heat flux hot channel factor: ratio of the maximum local fuel rod linear power density to the core average fuel rod linear power density, calculated as:

$$F_{(Q)}(Z) = F_{(xy)}(Z) \times \frac{average\ power\ density\ at\ elevation\ Z}{average\ core\ power\ density} \tag{24}$$

- Nuclear enthalpy rise hot channel factor: ratio of the integral of the linear power along the fuel rod with the highest integrated power to the average integrated fuel rod power, calculated as:

$$F_{(\Delta H)} = \frac{maximum\ of\ \sum_Z power}{average\ power} \tag{35}$$

A comparison of hot channel factors calculated using RELAP5-3D data and PARCS data is shown in Figure 31. The left-hand side shows the radial peaking factor at elevation Z, while the right-hand side shows the heat flux hot channel factor at elevation Z. Meanwhile, the nuclear enthalpy rise $F_{\Delta H}$ is a single value instead of a function of elevation. The $F_{\Delta H}$ calculated with RELAP5 is 1.3628 while $F_{\Delta H}$ calculated with PARCS is 1.3542. These comparisons affirm the excellent agreement between RELAP5-3D and PARCS.

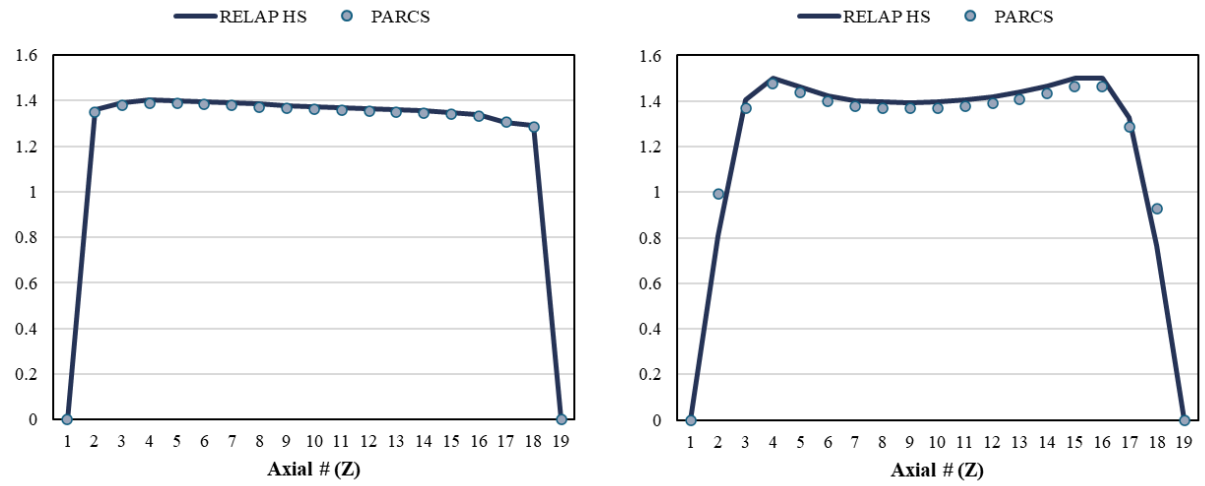

(a) (b)

Figure 31. Hot channel factors comparison between RELAP5-3D and PARCS.

Following the steady-state analysis, a reactivity insertion transient scenario was simulated in RELAP5-3D. In this scenario, a control rod was assumed to be ejected out of the core in 0.1 seconds, introducing a positive reactivity that increases power production. The control rod is located at coordinate E9, corresponding to the coolant channel number 842 in Figure 28. Snapshots of axial-averaged reactor core power during this reactivity transient are shown in Figure 32. The Figure shows a swift increase of power on the left-region of the core where the control rod is located, causing a localized increase of the peaking factors. This sample transient calculation demonstrates the capabilities of the computational platform that has been set up for the power uprate analysis. Future studies will involve the inclusion of more REA and operational transient cases, including a corresponding sensitivity and uncertainty analysis.

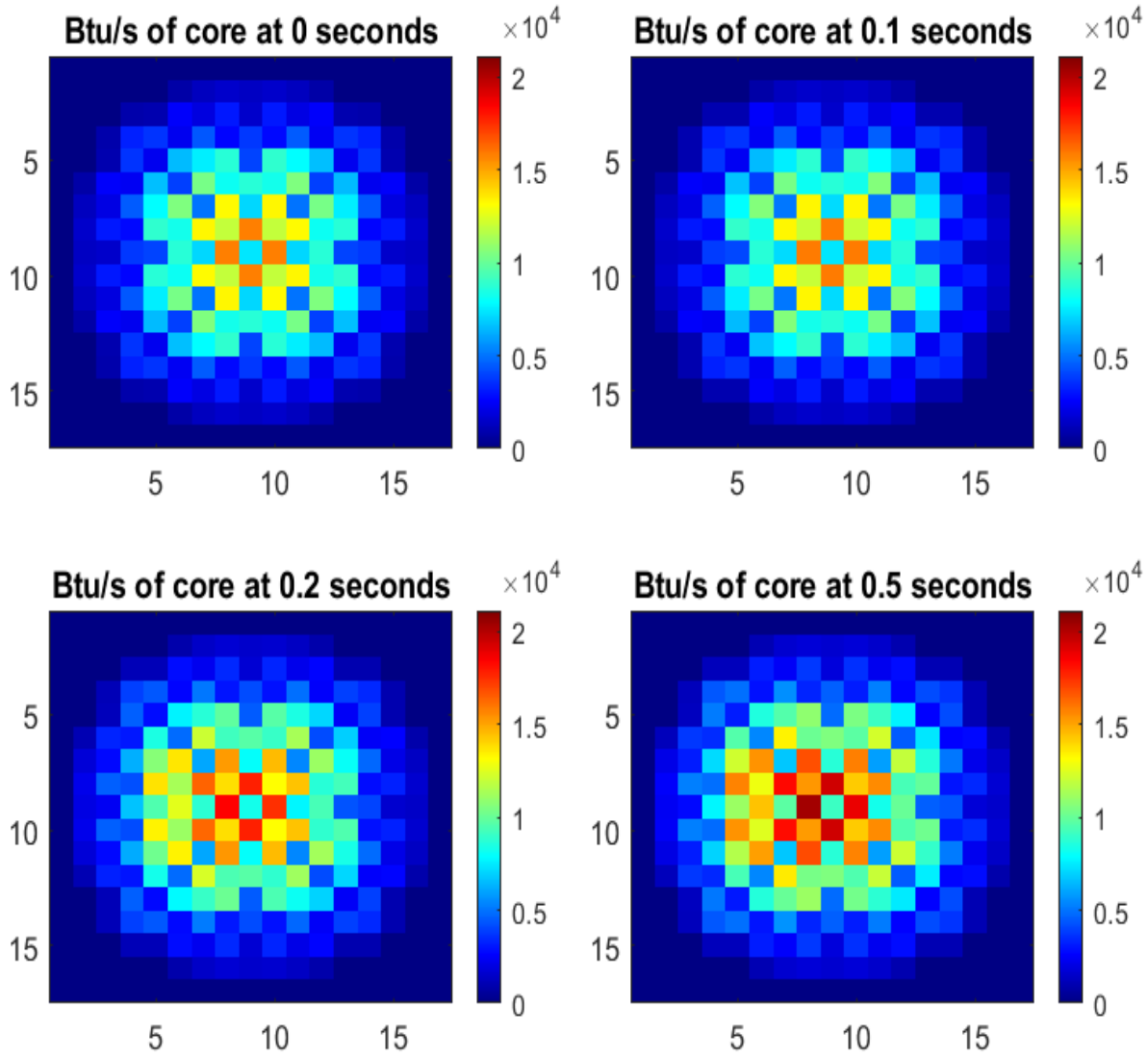

Figure 32. Reactor core power in Btu/s during control rod ejection.

3.2 RELAP5-3D–CTF Coupling for Subchannel Modeling

CTF is an updated version of COBRA-TF which stands for COolant Boiling in Rod Arrays-Two Fluids, which is a thermal-hydraulic simulation code specifically designed for analyzing LWR vessels. The software is currently managed by the Reactor Dynamics and Fuel Management Group (RDFMG) at North Carolina State University. CTF can be employed for thermal-hydraulic rod bundle analysis and LWR safety analysis, as well as for modeling transients such as LOCAs in PWRs. The code employs a two-fluid, three-field modeling approach, which includes fluid film, fluid drops, and vapor. Each field is governed by its own set of conservation equations, assuming the liquid and droplet fields are in thermal equilibrium, and thus share a common energy equation [17].

Coupling CTF with RELAP5-3D therefore allows for resolution of detailed thermodynamic variables at a subchannel level especially while modeling transients. CTF is also ideal for analyzing thermal-hydraulic performance of individual fuel bundles to get detailed temperature distributions and flow parameters. RELAP5-3D uses a coarse meshing scheme, which may not be able to capture accurate local conditions for the calculation and prediction of CHF. On the other hand, CTF uses a finer spatial

resolution to understand local boiling phenomena, coolant flow and heat transfer for individual subchannels. CTF also contains built-in models for the calculation of CHF leading to a more accurate prediction [3, 17].

Previous work has been performed to couple RELAP5-3D with NESTLE and CTF in a multiphysics engineering simulator. NESTLE and CTF were used to model the neutronics and thermal hydraulics, respectively, within the core on a fine mesh while RELAP5-3D modeled the entire nuclear steam supply system. In this work, RELAP5-3D provided the core boundary conditions to CTF while CTF provided a mesh-dependent coolant heating rate to the RELAP5-3D core solution. The work demonstrated that both CTF and RELAP5-3D provided similar steady-state core predictions as well as reasonable behavior during transient simulations, which indicated thermal-hydraulic compatibility between the two codes [18].

3.2.1 RELAP5-3D–CTF Coupling Methodology

The coupling of RELAP5-3D with CTF enables use of a higher fidelity subchannel code (CTF) to get thermodynamic variables on a finer mesh compared to a system code (RELAP5-3D) during a transient associated with control rod ejection. Figure 33 explains the methodology behind coupling RELAP5-3D with CTF [3, 17].

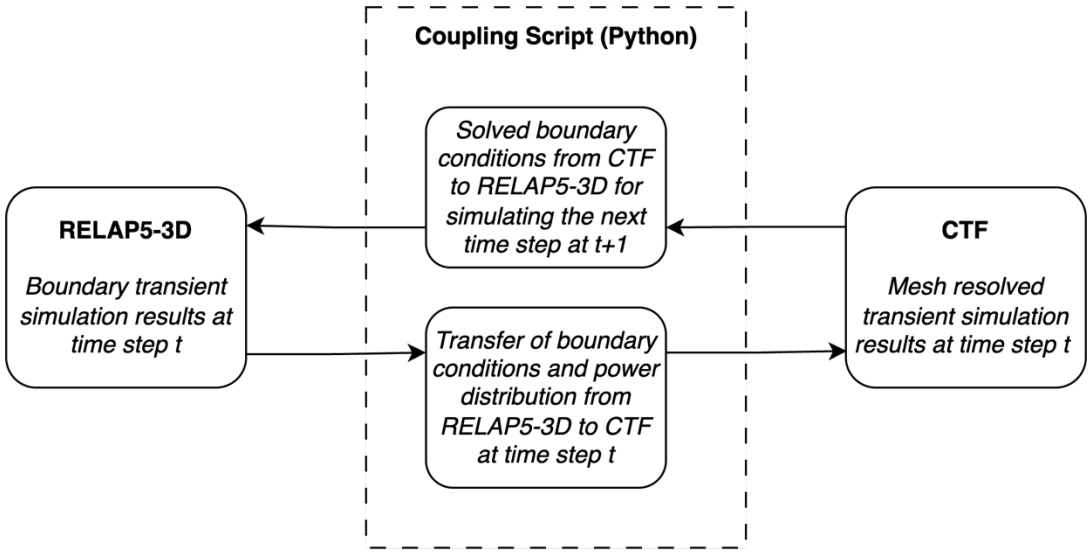

Figure 33. RELAP5-3D and CTF Coupling Methodology.

The following steps summarize the methodology for coupling RELAP5-3D and CTF during a control rod ejection transient where time step t ranges from the start of the transient $(t = 0)$ until the end of control rod ejection transient $(t = T)$.

1. RELAP5-3D is solved at time step t of the transient.
2. A coupling script, written in Python, takes the inlet and outlet boundary condition values of the reactor core that have been solved by RELAP5-3D, along with RELAP5-3D/NESTLE power distributions, and sends them to the CTF input file.
3. CTF is solved for time step t for the reactor core over different axial and radial nodes for the core. CTF also checks for the occurrence of critical heat flux during the particular time step t.
4. The coupling script written in Python uses the inlet and outlet boundary conditions solved by CTF at time step t as input to RELAP5-3D.
5. RELAP5-3D then simulates the next time step at $t + 1$ using the solved variables received from CTF.

6. This process is repeated until the end of the simulation when $t = T$. Throughout the simulation, thermodynamic variables, including those associated with CHF, are stored at each time step using the same coupling script. These variables are taken from the different output files created by CTF simulation.

The input variables sent to CTF from RELAP5-3D through the coupling script include thermodynamic variables at the inlet and outlet of the reactor core, excluding the plenum. These variables encompass the following:

- Inlet pressure (measured in bar)
- Outlet pressure (measured in bar)
- Inlet mass flow rate (measured in kg/s) through the entire core
- Inlet temperature (measured in °C) and/or enthalpy (measured in kJ/kg)
- Outlet temperature (measured in °C) and/or enthalpy (measured in kJ/kg)
- Rod power (measured in kW/ft).

Additionally, if given pressure and temperature values, steam tables can be incorporated into the coupling script to compute the enthalpy. After these variables are sent to the CTF input file, CTF is simulated using their built-in convergence criteria. CTF also checks for the occurrence of CHF for the simulation at time step t using inbuilt CHF correlations. After the CTF simulation ends, updated inlet and outlet boundary condition variables from CTF are sent back to RELAP5-3D to simulate the next time step $(t + 1)$. These variables include thermodynamic variables, like inlet and pressure and inlet and outlet temperature.

3.2.2 Plans for Validation of the Coupling Methodology

As a use case to apply the coupling methodology mentioned in Section 3.2.1, a simplified CTF model was created. This simplified CTF model is described as:

1. A single rod is simulated in CTF as a simplified core. It is assumed that radial power throughout the core is homogenized and, thus, a single rod can be simulated using the CTF input file.
2. This single rod is surrounded by four subchannels each with a cross-sectional area of 2.26020E-05 m^2.
3. The physical parameters of the single rod are as follows:
    a. Length of fuel rod = 3.658 m
    b. Diameter of fuel rod = 0.0095 m
    c. Diameter of fuel = 0.008192 m
    d. Thickness of clad = 5.70000E-04 m
4. The length of the fuel rod is discretized into 49 nodes.
5. It is assumed that the axial power profile is uniform.
6. CTF has the ability to use the following variable combinations as boundary conditions:
    a. Pressure and enthalpy/temperature
    b. Mass flow rate and enthalpy/temperature
    c. Mass flow rate only
    d. Mass source (mass flow rate and enthalpy)

e. Pressure sink (pressure and enthalpy)

f. Mass flow rate, void, and slip ratio (only works for inlet).

In the input file, pressure, mass flow rate, and temperature values are used to define the inlet boundary condition, and pressure and temperature values are used to define the outlet boundary condition.

7. CTF has three built-in models to compute CHF: the W3 correlation, Bowring correlation, and Groeneveld look-up table. The present use-case input file makes use of the W3 correlation for CHF calculation.
8. The following variables are sent by the coupling script from RELAP5-3D to CTF:
    a. Total mass flow rate in kg/s
    b. Linear heat generation rate in kW/m
    c. Initial pressure in fluid domain in bar
    d. Initial temperature in °C or enthalpy in kJ/kg as inlet boundary condition
    e. Outlet temperature in °C or enthalpy in kJ/kg
    f. Outlet pressure in bar.

This simplified design is then simulated using the input file, with CTF using the internal code convergence criteria. The simulation results get saved in multiple text files and hdf5 files. These files are then read by the coupling script that pull out the needed boundary conditions like inlet and outlet temperatures, pressures, and enthalpies to be sent to RELAP5-3D along with CHF information.

3.2.3 Results and Future Steps

The use case for the simplified single-rod case will serve as a preliminary test of the coupling methodology. For the single-rod framework, it is assumed that the thermal power is normalized across the fuel rods in one assembly, requiring only one rod to be modeled in CTF. This serves as an economical means of validating the successful transfer of information from RELAP5-3D to CTF using the established coupling methodology in the prepared coupling script. This framework can be useful in determining the necessary data to be read from the output files generated to CTF to transfer the boundary conditions to RELAP5-3D. This framework can then be further developed to model an entire assembly and then the entire core to incrementally improve the fidelity of the coupling framework. This can help in understanding which assembly and rod are prone to CHF. It would then be possible to get local coolant flow and heat transfer properties for every subchannel in each assembly of the core.

To model entire assemblies of the core, CTF would require the following additional information:

1. Pin-resolved power factors within assembly and core
2. Core and assembly dimensions
3. Rod configurations
4. Guide tube dimensions
5. Number of spacer grids
6. Fuel composition
7. Axial power distribution
8. Grid loss coefficient data.

Thus, this use-case framework can be developed for full assemblies and core. This information can help determine in which fuel rods and assemblies CHF could occur throughout the control rod insertion transient.

4. SUMMARY AND FUTURE WORK

The aim of this project was to conduct a feasibility study for a significant power uprate in a PWR by using low 5%–10% enrichment uranium (LEU+) fuel at high burnup. In FY-25, R&D efforts focused on demonstrating the application of an extended power uprate to the high-fidelity core model of an existing LWR core design operating in the U.S., specifically the STP reactor core. The work presented by this report is part of a broader initiative by the U.S. government to increase nuclear energy capacity as a key aspect of the nation's energy strategy. The study's primary goals were to achieve a significant power uprate from 3800 MWth to 4500 MWth and to extend the fuel cycle length from 18 months (530 EFPD) to 24 months (700 EFPD).

PARCS was employed to perform core transport calculations before and after the application of the extended power uprate, ensuring the study's relevance to the nuclear industry and accelerating the licensing process with the identified optimal design approach. Fuel assembly models were created in POLARIS to generate a multiparametrized cross-section library with the addition of LEU+ fuel and urania-gadolinia burnable poisons to support the significant increase in thermal power (18%). The STP Unit 1 reactor core was then optimized to support the extended power uprate and to include the new LEU+ fuel designs. The resulting equilibrium cycle core configuration meets all of the design criteria of the extended power uprate, while also satisfying various operational and safety constraints, such as thermal power peaking factors and peak soluble boron concentration in the coolant. A reactor system model was developed using RELAP5-3D with nodal kinetics calculations based on the NESTLE module. The reactor model is a typical four-loop PWR based on the STP nuclear power plant. A methodology was developed to automatically generate the three-dimensional neutron kinetic input deck, using as input the neutron cross section database from POLARIS and the core optimized configurations derived by PARCS. A sample transient system model of an REA was also created to analyze an example of a non-symmetric and strongly localized power perturbation. Moreover, the coupling strategy between RELAP5-3D and subchannel code CTF have been identified and described.

Continued work is expected to be necessary to accomplish the broader goals of this study; namely, improving the foundation of the U.S. nuclear energy sector in accordance with the stated goals of the U.S. government. This future work will include AOO- and DBA-transient scenarios that could be quickly analyzed in the coming fiscal year. The results of such scenarios will provide information about whether safe operation parameters are fulfilled under different operational conditions and accident scenarios, combining the best estimate analysis from the developed computational platform with the uncertainty analysis from the RAVEN code. These future activities, based on the so-called best estimate plus uncertainty (BEPU) methodologies, will allow a more precise identification of the safety margins of the new power-uprated cores. Future work will also focus on improving the coupling of multiphysics simulations that integrate reactor physics and thermal hydraulics, both at the system and subchannel levels, for a more comprehensive understanding of power uprate impacts. In addition, applying the extended power uprate methodology to other existing LWRs beyond the STP Unit 1 reactor will involve adapting the developed models and findings to different reactor designs and configurations and conducting economic feasibility studies to evaluate the cost-effectiveness of implementing such power uprates across the U.S. nuclear fleet to inform the decision-making process for future reactor upgrades.

Finally, the activities described in this report will be relevant for the future time-at-temperature research activities. As the industry moves toward higher energy density cores, the probability of having thermal crisis and time-at-temperature events during an AOO or a DBA will increase. The planned time-at-temperature research activities will help better understand this phenomenon, resulting in reduced

uncertainties for the fuel performance and for the thermal-hydraulic codes predictions. At the same time, the optimized cores and the computational platform and methods described in this report will provide a reference testbed for the industry for the realistic simulation of time-at-temperature events.

ACKNOWLEDGEMENT

This research made use of Idaho National Laboratory's High Performance Computing systems located at the Collaborative Computing Center and supported by the Office of Nuclear Energy of the U.S. Department of Energy and the Nuclear Science User Facilities under Contract No. DE-AC07-05ID14517.

5. REFERENCES

1. Federal Register, Executive Order 14300, *Ordering the Reform of the Nuclear Regulatory Commission.* 2025, The White House: Washington, D.C.
2. Federal Register, Executive Order 14302, *Reinvigorating the Nuclear Industrial Base*. 2025, The White House: Washington, D.C.
3. *RELAP5-3D Code Manual Volume I: Code Structure, System Models and Solution Methods, INL-EXT-98-00834, Rev. 4.1*. 2013, Idaho National Laboratory: Idaho Falls, ID, USA.
4. *Power Uprates for Nuclear Plants*. 2022, Nuclear Regulatory Comission.
5. T. Downar, Y.X., and V. Seker, *PARCS v3.0 U.S. NRC Core Neutronics Simulator User Manual (UM-NERS-09-0001)*. 2010, University of Michigan.
6. Turinsky, P.J., et al., *NESTLE: Utilzing the Nodal Expansion Method For Eigenvalue, Few-Group Neutron Diffusion Equation Solver Adjoint, Fixed-Source Steady-State and Transient Problems*. 1994, Electric Power Research Center, North Carolina State University.
7. *TRACE V5.0 PATCH 5 MANUAL*. 2017, US Nuclear Regulatory Commission.
8. *Boric Acid Corrosion of Carbon Steel Reactor Pressure Boundary Components in PWR Plants (Generic Letter 88-05)*. 1988, U.S. Nuclear Regulatory Commission.
9. Stacey, W.M., *Nuclear Reactor Physics*. 2001: Wiley-Interscience.
10. *Integral Fuel Burnable Absorber (IFBA) Fuel Cycles and IFBA/Gad Hybrid Fuel Cycles (NFCM-0015) Rev. 1*. 2018, Westinghouse Electric Company LLC.
11. Hida, K., T. Ikehara, and K. Nittoh, *Nuclear fuel containing gadolinium*. 1996.
12. S. Yilmaz, K.I., S. Levine, and M. Mahgerefteh, *Development of enriched Gd-155 and Gd-157 burnable poison designs for a PWR core.* Annals of Nuclear Energy, 2006. **33**(5): p. 439-445.
13. M. A. Jessee, W.A.W., T. M. Evans, S. P. Hamilton, J. J. Jarrell, K. S. Kim, J. P. Lefebvre, and U.M. R. A. Lefebvre, A. B. Thompson, and M. L. Williams, *POLARIS: A new two dimensional lattice physics analysis capability for the SCALE code system*, in *PHYSOR 2014 - The Role of Reactor Physics toward a Sustainable Future*. 2014: Kyoto, Japan.
14. *Higher Burnup*. 2024, Nuclear Regulatory Commission.
15. *South Texas Project Units 1 and 2 - Updated Final Safety Analysis Report (Rev.18) - Chapter 4 REACTOR*. 2016, STP Nuclear Operating Company.
16. Lawrence, S., et al., *Development of New Reactor Core Configuration for Power Uprate – Fuel Reload and Heat Processing Analyses, Core Design, System Safety Assessments, and Fuel Performance Analyses (INL/RPT-24-80710)*. 2024, Idaho National Laboratory.
17. Salko, R.K. and M.N. Avramova, *CTF Theory Manual*. 2016, Pennsylvania State University, Department of Mechanical and Nuclear Engineering, Reactor Dynamics and Fuel Management Group.
18. Wysocki, A.J., R.K. Salko, and I. Arshavsky, *Coupling of CTF and RELAP5-3D Within an Enhanced-Fidelity Nuclear Power Plant Simulator.* Nuclear Technology, 2023. **209**(10): p. 1466-1484.
19. STPEGS UFSAR Chapter 4, Rev. 18, retrieved from U.S. NRC ADAMS online database, ML16207A543.

Page intentionally left blank

APPENDIX A – CTF Coupling Input File

```
**********************************************************************************
**********
*MAIN CONTROL DATA
**********************************************************************************
**********
*ICOBRA
    1
*INITIAL   DUMPF
     1      0
**   EPSO    OITMAX    IITMAX   COURANT
 0.001000        5        40  0.800000
*TITLE
Single Rod PSBT
**********************************************************************************
**********
*GROUP 1 - Calculation Variables and Initial Conditions                          *
**********************************************************************************
**********
**NGR
  1
**NGAS IRFC EDMD IMIX ISOL         GINIT NOTRN MESH MAPS IPRP MFLX NM12 NM13
NM14
   1   2   0   0   0          {G}     1   1   1   0   0   0   0   0
*Card 1.2
**         GTOT         AFLUX        DHFRAC         MFLUX
         {G}          {H}       0.0000000E+00.      0.0
*Card 1.3
**         PREF           HIN          HGIN           VFRAC1      VFRAC2      BRIN  RDIF
      {P_init}         {-Temp}       288.4200000   1.0000000    0.9999000    1000  0.0
*Card 1.4
**GTP(1)   VFRAC(3)  GTP(2) VFRAC(4)  GTP(3) VFRAC(5)  GTP(4) VFRAC(6)
   air     0.0001
**********************************************************************************
**********
*GROUP 2 - Channel Description                                                   *
**********************************************************************************
**********
**NGR
   2
*Card 2.1
**  NCH NDM2 NDM3 NDM4 NDM5 NDM6 NDM7 NDM8 NDM9 NM10 NM11 NM12 NM13
NM14
    4   0   0   0   0   0   0   0   0   0   0   0   0   0
*Card 2.2
**   I         AN         PW ABOT ATOP NMGP          X          Y        XSIZ       YSIZ
```

```
    1 2.26020E-05 7.46128E-03    0    0    0 -3.17500E-03  3.17500E-03  6.35000E-03  6.35000E-03
    2 2.26020E-05 7.46128E-03    0    0    0  3.17500E-03  3.17500E-03  6.35000E-03  6.35000E-03
    3 2.26020E-05 7.46128E-03    0    0    0 -3.17500E-03 -3.17500E-03  6.35000E-03  6.35000E-03
    4 2.26020E-05 7.46128E-03    0    0    0  3.17500E-03 -3.17500E-03  6.35000E-03  6.35000E-03
*******************************************************************************************
**********
*GROUP 3 - Transverse Channel Connection (Gap) Data
*******************************************************************************************
**********
**NGR
   3
*Card 3.1
**  NK NDM2 NDM3 NDM4 NDM5 NDM6 NDM7 NDM8 NDM9 NM10 NM11 NM12 NM13 NM14
    4   0    0    0    0    0    0    0    0    0    0    0    0    0
*Card 3.2
**   K    IK    JK         GAP         LNGT    WKR FWAL IGPB IGPA FACT IG JG IG JG IG JG
*Card 3.3
**GMULT   ETNR
    1    1    2  1.60000E-03  8.16743E-03 0.50 0.00    0    0  1.0  0  0  0  0  0  0
     1    0.0
    2    1    3  1.60000E-03  8.16743E-03 0.50 0.00    0    0  1.0  0  0  0  0  0  0
     1    0.0
    3    2    4  1.60000E-03  8.16743E-03 0.50 0.00    0    0  1.0  0  0  0  0  0  0
     1    0.0
    4    3    4  1.60000E-03  8.16743E-03 0.50 0.00    0    0  1.0  0  0  0  0  0  0
     1    0.0
*Card 3.3.5
**   K           X           Y      NORM
    1  0.00000E+00  0.31750E-02     x
    2 -0.31750E-02  0.00000E+00     y
    3  0.31750E-02  0.00000E+00     y
    4  0.00000E+00 -0.31750E-02     x
*Card 3.4
**NLGP
    0
*******************************************************************************************
**********
*GROUP 4 - Vertical Channel Connection Data                                          *
*******************************************************************************************
**********
**NGR
   4
*Card 4.1
**NSEC NSIM IREB NDM4 NDM5 NDM6 NDM7 NDM8 NDM9 NM10 NM11 NM12 NM13 NM14
    1    1    0    0    0    0    0    0    0    0    0    0    0    0
*Card 4.2
**ISEC    NCHN  NONO        DXS     IVAR
```

```
   1      4    49 7.46449E-02      49
*Card 4.3
**JLEV       VARDX  JLEV       VARDX  JLEV       VARDX  JLEV       VARDX  JLEV
VARDX
   2 3.8660000E-02    3 8.2110000E-02    4 8.2110000E-02    5 8.2110000E-02    6 8.2120000E-02
   7 8.2110000E-02    8 8.2110000E-02    9 8.2110000E-02   10 3.8100000E-02   11 8.0650000E-02
  12 8.0650000E-02   13 8.0650000E-02   14 8.0650000E-02   15 8.0650000E-02   16 8.0650000E-02
  17 3.8100000E-02   18 8.0650000E-02   19 8.0650000E-02   20 8.0650000E-02   21 8.0650000E-02
  22 8.0650000E-02   23 8.0650000E-02   24 3.8100000E-02   25 8.0650000E-02   26 8.0650000E-02
  27 8.0650000E-02   28 8.0650000E-02   29 8.0650000E-02   30 8.0650000E-02   31 3.8100000E-02
  32 8.0650000E-02   33 8.0650000E-02   34 8.0650000E-02   35 8.0650000E-02   36 8.0650000E-02
  37 8.0650000E-02   38 3.8100000E-02   39 8.0650000E-02   40 8.0650000E-02   41 8.0650000E-02
  42 8.0650000E-02   43 8.0650000E-02   44 8.0650000E-02   45 3.8100000E-02   46 7.9212000E-02
  47 7.9212000E-02   48 7.9212000E-02   49 7.9212000E-02   50 7.9212000E-02
*Card 4.4
**   I  KCHA  KCHA  KCHA  KCHA  KCHA  KCHA   KCHB  KCHB  KCHB  KCHB  KCHB  KCHB
    1    1    0    0    0    0    0    1    0    0    0    0    0
    2    2    0    0    0    0    0    2    0    0    0    0    0
    3    3    0    0    0    0    0    3    0    0    0    0    0
    4    4    0    0    0    0    0    4    0    0    0    0    0
*Card4.5
**  IWDE
     4
*Card 4.6
**  MSIM
    196
*************************************************************************************
**********
*GROUP 7 - Grid Loss Coefficient Data                                              *
*************************************************************************************
**********

*************************************************************************************
**********
*GROUP 8 - Rod and Unheated Conductor Data                                         *
*************************************************************************************
**********
**NGR
   8
*Card 8.1
** NRRD   NSRD    NC  NRTB  NRAD  NLTY  NSTA   NXF  NCAN  RADF    W3 IHTC  DNBCHK
NDM14
    1    0    3    1    0    0    1    1    0    0    1    1    1    0
*Card 8.2
**    N  IFTY   IAXP   NRND DAXMIN  RMULT       HGAP  ISECR  HTAMB   TAMB  SYMROD
*Card 8.3
```

```
**NSCH   PIE  NSCH   PIE  NSCH   PIE  NSCH   PIE  NSCH   PIE  NSCH   PIE  NSCH   PIE NSCH
PIE
    1     1     1     0     0  1.000 5.67830E+03     1  0.000  0.000   1.000
   3 0.250    4 0.250    1 0.250    2 0.250    0 0.000    0 0.000    0 0.000    0 0.000
*Card 8.6
**   I  NRT1   NST1   NRX1
    1     1     0     2
*Card 8.7
**IRTB1  IRTB2  IRTB3  IRTB4  IRTB5  IRTB6  IRTB7  IRTB8  IRTB9 IRTB10 IRTB11 IRTB12
    1
*Card 8.9
**    AXIALT      TRINIT
 0.00000E+00     {Temp_in}
 0.36580E+01     {Temp_out}
**********************************************************************************
**********
*GROUP 9 - Conductor Geometry Description                                        *
**********************************************************************************
**********
**NGR
   9
*Card 9.1
** NFLT IRLF ICNF IMWR NDM5 NDM6 NDM7 NDM8 NDM9 NM10 NM11 NM12 NM13 NM14
    1   0   0   0   0   0   0   0   0   0   0   0   0   0
*Card 9.2
**  I FTYP       DROD       DFUL  NFUL IMTF IMTC IMOX DCRE        TCLD    FTDS IGPC IGFC
IRDP
   1 nucl 0.00950000 0.00819200     3    0    0    0 0.00 5.70000E-04 0.95000    0    0    0
**********************************************************************************
**********
*GROUP 10 - Material Properties Tables                                           *
**********************************************************************************
**********
**********************************************************************************
**********
*GROUP 11 - Core Power Distribution Information                                  *
**********************************************************************************
**********
**NGR
  11
*Card 11.1
** NQA  NAXP  MNXN    NQ  NGPFF   NQR  NDM7  NDM8  NDM9 NDM10 NDM11 NDM12
NDM13 NDM14
    1    1    2    0    0    1    0    0    0    0    0    0    0    0
*Card 11.2
**         YQA
   0.00000E+00
```

```
*Card 11.3
**   I  NAXN
    1     2
*Card 11.4
**         Y      AXIALZ
  0.00000000  1.00000000
  3.65800000  1.00000000
*Card 11.5
** YQ  FQ
*Card 11.7
**          YQR
   0.00000E+00
*Card 11.8
**    FQR1      FQR2      FQR3      FQR4      FQR5      FQR6      FQR7      FQR8
     1.0000

*************************************************************************************
**********
*GROUP 12 - Turbulent Mixing and Void Drift Data
*************************************************************************************
**********
**NGR
*   12
*Card 12.3
*    AAAK      BETA      THETM
 0.140E+01 0.500E-01 0.500E+01
*************************************************************************************
**********
*GROUP 13 -  Boundary Condition Data                                          *
*************************************************************************************
**********
**NGR
   13
*Card 13.1
** NBND   NKBD NFUN NGBD VBC  NDM6 NDM7 NDM8 NDM9 NM10 NM11 NM12 NM13
NM14
     8     0   0   0   0   0   0   0   0   0   0   0   0   0
*Card 13.4
**Inlet b.c. ----------------------------------------------------------
** IBD1   IBD2 ISPC N1FN N2FN N3FN     BCVALUE1     BCVALUE2     BCVALUE3 INITGAS
     1      1   2    0    0    0  0.00000E+00     {-Temp}     0.00000E+00       1
     2      1   2    0    0    0  0.00000E+00     {-Temp}     0.00000E+00       1
     3      1   2    0    0    0  0.00000E+00     {-Temp}     0.00000E+00       1
     4      1   2    0    0    0  0.00000E+00     {-Temp}     0.00000E+00       1
**outlet b.c. ---------------------------------------------------------
     1     57   1    0    0    0  0.00000E+00     {h}      {P_init}          1
     2     57   1    0    0    0  0.00000E+00     {h}      {P_init}          1
```

```
    3    57   1   0   0   0  0.00000E+00   {h}     {P_init}        1
    4    57   1   0   0   0  0.00000E+00   {h}     {P_init}        1
*******************************************************************************
**********
*GROUP 14 - Output Options
*******************************************************************************
**********
**NGR
 -14
**     KEY     VALUE
     hdf5        1
   rod_vtk        0
 chan_edits        1
  rod_edits        1
  gap_edits        0
  fluid_vtk        1
  dnb_edits        1
convergence        1
end 14
*******************************************************************************
**********
*GROUP 15 - Time Domain Data
*******************************************************************************
**********
**NGR
  15
*Card 15.1
 1.0000E-06  1.0000E-01  1.0000E-01  0.0000E+00  0.0000E+00     1.000000e+02      10000
*******************************************************************************
**********
*GROUP 17 - Channel/Rod Maps for HDF5 and VTK files
*******************************************************************************
**********
**NGR
  17
*Card 17.1 - HDF5_NAME VTK_NAME
single_rod_HFP.hdf5          single_rod_HFP.vtk
*Card 17.2 - Rod Map Dimensions
**TOTRODSROW TOTRODSCOL
         1         1
*Card 17.3 - Channel Map Dimensions
**TOTCHANSROW TOTCHANSCOL
         2         2
*Card 17.4 - Rod Map
   1
*Card 17.4 - Channel Map
   1   1
```

```
   1    1
{assem map}
** sym_opt  nassem_rows  nassem_cols
      1           1           1
**Assembly Map
   1
*******************************************************************************
**********
*GROUP 18 - convergence Criteria for Steady State Solve
*******************************************************************************
**********
**NGR
  18
*Card 18.1
**Global Energy Balance Criteria (%)
 0.010000
*Card 18.2
**Global Mass Balance Criteria (%)
 0.010000
*Card 18.3
**Fluid Energy Storage Criteria (%)
 0.500000
*Card 18.4
**Solid Energy Storage Criteria (%)
 0.500000
*Card 18.5
**Mass Storage Criteria (%)
 0.500000
```